TRIBHUVAN UNIVERSITY

INSTITUTE OF ENGINEERING

PULCHOWK CAMPUS

THESIS NO: M-71-MSMDE-2021-2023

STUDY OF CORRELATION BETWEEN CAVITATION AND SEDIMENT EROSION IN FRANCIS TURBINE

by

NAVIN BHATT

A THESIS
SUBMITTED TO THE DEPARTMENT OF MECHANICAL AND AEROSPACE ENGINEERING IN PARTIAL FULFILLMENT OF THE REQUIREMENTS FOR THE DEGREE OF MASTERS OF SCIENCE IN MECHANICAL SYSTEM DESIGN AND ENGINEERING

DEPATRMENT OF MECHANICAL AND AEROSPACE ENGINEERING
LALITPUR, NEPAL

NOVEMBER, 2023

COPYRIGHT

TRIBHUVAN UNIVERSITY

INSTITUTE OF ENGINEERING

PULCHOWK CAMPUS

DEPARTMENT OF MECHANICAL AND AEROSPACE ENGINEERING

This is to verify that the thesis entitle **"STUDY OF CORRELATION BETWEEN CAVITATION AND SEDIMENT EROSION IN FRANCIS TURBINE"** submitted by **Mr. Navin Bhatt (PUL078MSMDE010)** has been examined and is accepted, in partial fulfillment of the requirements for the degree of Masters in Science in Mechanical System Design and Engineering of Tribhuvan University.

Prof. Dr. Laxman Poudel,
Supervisor,
Department of Mechanical and Aerospace Engineering

Asst. Prof. Dr. Sudip Bhattarai,
Supervisor,
HOD of Mechanical and Aerospace Engineering

Junior. Prof. Er. Anil Sapkota,
External Examiner,
Nepal Engineering College

Prof. Dr. Laxman Poudel
Program Coordinator,
Department of Mechanical and Aerospace Engineering

Tribhuvan University
Institute of Engineering
Department of Mechanical and Aerospace Engineering
Pulchowk Campus

Committee Chairperson,
Asst. Prof. Dr. Sudip Bhattarai,
HOD of Mechanical and Aerospace Engineering

Date: 26 /11/2023

ABSTRACT

Cavitation in reaction turbines is undesirable and more vulnerable, presenting challenges such as vibration, performance degradation, and damage to hydraulic turbine components in hydropower plants. In Nepal, the Himalayan Rivers generate substantial sediment with hard abrasive particles, posing a hindrance to the economic development of hydropower resources. The current study employs numerical analysis to investigate the effects of cavitation and sediment, as well as the correlation between these two factors in a Francis turbine. The SST k-omega turbulence model is utilized to address fluid turbulence phenomena, and computational fluid dynamics (CFD) techniques are applied through ANSYS-Fluent software to explore the performance characteristics related to sediment and cavitation erosion in a hydraulic Francis turbine. For erosion rate calculations, the Tabakoff–Grant particle trajectory erosion model is employed. The study predicts cavitation characteristics using the Schnerr and Sauer cavitation model for interphase mass transfer. Furthermore, the Multi-phase Dense Discrete Phase model is chosen to examine the combined impact of cavitation and sediment erosion in ANSYS-Fluent. The study investigates three distinct operating conditions under the effects of cavitation and sediment erosion, namely part load, Best Efficiency Point (BEP), and full load conditions. Results are presented in terms of pressure fluctuation, vapor volume fraction, mass transfer, and erosion rate density. Simulations indicate the presence of low-pressure regions at the suction side of the runner blade, leading to the formation of high vapor bubbles and subsequent cavitation effects. The highest erosion is predicted at the trailing edge on the pressure side of the runner blade surface, with a maximum erosion rate density on the runner of 2.27E-08 $kgm^{-2}s^{-1}$ during full load conditions compared to BEP and part load. Additionally, the combined condition estimates an erosion rate density on runners of 7.52E-05 $kgm^{-2}s^{-1}$, which is 4.61×10^{3} times higher than the erosion rate density when examining the effect of sediment erosion only at BEP. Consequently, the study using Multi-phase Dense Discrete Phase model reveals that the trailing edge of the blade profile is significantly affected by sediment-water-vapor along both the suction and pressure sides, resulting in material loss at that location.

ACKNOWLEDGMENTS

First and foremost, I am greatly thankful to our Mechanical & Aerospace Engineering Department, Pulchowk Campus, TU for providing me the opportunity to carry out this project on “Study of correlation between cavitation and sediment erosion in Francis turbine”. I would like to express my sincere gratitude to my supervisor **Prof. Dr. Laxman Poudel & Assist. Prof. Sudip Bhattarai** for his expert advice, guidance and meticulous encouragement from the beginning to the end to complete this work.

Additionally, I would like to express my heartfelt gratitude to **Mr. Binod Pandey**, an NEA Engineer currently engaged at the Kali Gandaki "A" Hydroelectric Project (144 MW), Nepal, for giving valuable information and photographs of an eroded runner which are essential for the completion of this study.

My heartfelt gratitude goes to countless reader of this project report, who is the most important critic and commentator. I welcome constructive comments and suggestions which will help us to do better one.

At last I would like to thank those people who gave their helping hands directly or indirectly for this project

TABLE OF CONTENTS

LIST OF FIGURES

LIST OF TABLES

LIST OF SYMBOLS

Symbol	Definition/Term	Units
A	Cross Sectional Area	m^2
D	Diameter	m
$\boldsymbol{\sigma}$	Thoma cavitation coefficient	-
$\boldsymbol{\sigma_c}$	Critical Cavitation Coefficient	-
$\boldsymbol{\rho}$	Density	Kg/m^3
$\mathbf{H_a}$	Atmospheric Pressure Head	m
$\mathbf{H_s}$	Suction Pressure Head	m
$\mathbf{H_v}$	Vapor Pressure Head	m
Q	Flow rate	m^3/s
$\boldsymbol{P_v}$	Liquid vapor pressure	Pascal
$\boldsymbol{r_b}$	Bubble radius	m
$\boldsymbol{E_{vap}}$	Evaporation coefficient	-
$\boldsymbol{k}$	Turbulent kinetic energy	Joule
$\boldsymbol{\omega}$	Angular Velocity	rad/sec
$\boldsymbol{\mu_t}$	Turbulent viscosity	Pascal_sec
$\boldsymbol{a, r, t}$	Axial, radial & tangential components	-
$\boldsymbol{\tau}$	Torque	N_m
$\boldsymbol{g}$	Acceleration due to gravity	m/s^2

LIST OF ACRONYMS AND ABBREVIATIONS

ANSYS	Analysis Systems
CFD	Computational Fluid Dynamics
ROR	Run-off-River
RDA	Rotary Disc Apparatus
HVOF	High Velocity Oxygen Fuel
JHC	Jhimruk Hydroelectric Centre
DDPM	Dense Discrete Phase Model
VOF	Volume of Fluid
DEM	Discrete Element Method
SST	Shear Stress Transport
E-L	Eulerian-Lagrangian
FEM	Finite Element Method
GV	Guide Vane
HEP	Hydroelectric Project
MW	Mega Watt
RPM	Revolutions Per Minute

CHAPTER 1 INTRODUCTION

1.1 Background

Nepal possesses significant hydropower energy potential due to its ownership of over six thousand rivers and its favorable geographical conditions for the establishment of hydropower plants. The country's topography and water runoff make it abundantly rich in hydropower, with the potential to generate up to 83,000 megawatts (MW) of electricity (Mukhia, 2021). Nepal is thought to possess the technical and financial capacity to develop hydroelectric generation power exceeding 43,000 MW. Nonetheless, the installed power as of right now is about 2,684 MW (Lama, 2018) (NEA, 2022/2023).

Erosion and sedimentation are greatly aided by the climatic and physical characteristics of the Himalayan Rivers region. Almost 6 billion tons of Earth's resources are carried to sea each year by the Indian subcontinent alone, out of an estimated 20 billion tons total. Moreover, Nepal's Karnali River has an exceptionally high specific sediment output., amounting to 4363 tons per square kilometer per year, which surpasses the sediment production in other major watersheds like the Yellow River in China (2470 tons per square kilometer per year)(Thapa, 2004). The significant sediment levels in such rivers can be attributed to factors such as the existence of fragile rocks, steep terrain, and intense rainfall during the monsoon. As a result, sediment management has emerged as a matter of paramount significance for ensuring the durability, dependability, and safety of the region's infrastructure. Despite the implementation of sediment trapping systems, it is neither feasible nor cost-effective to entirely remove fine sediment from the water. Consequently, most turbine parts in the rivers of the Himalayas remain uncovered by water laden with sand, making them susceptible to erosion. This erosion, in turn, leads to reduced efficiency and a shorter lifespan for the turbines.

The turbine serves as the central component of any hydropower plant, responsible for the conversion of potential energy into electrical energy. Turbines are categorized into two main types, impulse, and reaction, based on how water interacts with the runner of the turbine. Among these, Francis turbines, which fall under the category of reaction turbines, prove to be ideal for hydropower facilities of any size. This kind of turbine finds application covering power levels of from 0.25 to 800 megawatts per unit with a head range that normally spans from roughly 15 meters to 750 meters. Turbine components perform worse after a few years of use, even though they are still functional. This decline

is primarily attributed to various factors, including faults in the material, fatigue, cavitation, and silt erosion, which lead to damage and reduced efficiency over time.

Cavitation in hydraulic machinery leads to undesirable consequences, including flow instabilities, excessive vibrations, surface damage to materials, and a decline in machine performance. Regrettably, these issues are gaining prominence due to the increasing likelihood of cavitation. There are two primary reasons for this escalation. Firstly, the drive to boost power output of the turbine hinges on shrinking dimensions in order to save component costs. As a result, speeds are being raised, resulting in the cavitation number dropping, and thereby increasing the risk of cavitation. Secondly, a trend has emerged in which turbines are operated under conditions significantly deviating from their ideal efficiency points. This deviation is often driven by the market for hydropower generating being deregulated. Consequently, when operating outside of design, the likelihood of cavitation phenomenon increasing. The amalgamation of these two elements undoubtedly heightens the possibility of cavitation issues in hydraulic machinery.

Figure 1. 1 Cavitation damage on the blades at the discharge from a Francis turbine (Brennen, 2011)

Components of hydropower turbines eroded by sediment poses a significant challenge, primarily because the rivers in the Andes and Himalayas contain hard particles. Quartz, feldspar, and other hard minerals are the main ingredients in these areas. These particles have a Moh's hardness level of more than 5, which means they can erode turbine parts. This erosion causes decreased plant efficiency when the plant is operating in addition to causing problems with turbine maintenance.

When it comes to Francis turbines, erosion is mostly seen in places like the runner blades, stay vanes, and guiding vanes. The degree and configuration of erosion depend on the operational parameters and the particular flow phenomena in different areas. Francis turbine flow characteristics are frequently quite erratic, especially near the guiding vanes and runners. (Chitrakar, 2018).

In order to mitigate erosion in turbine components, it would be highly beneficial to predict the areas susceptible to erosion. This predictive insight can prove invaluable in the advancement of coating methods and the improvement of turbine component hydraulic design.

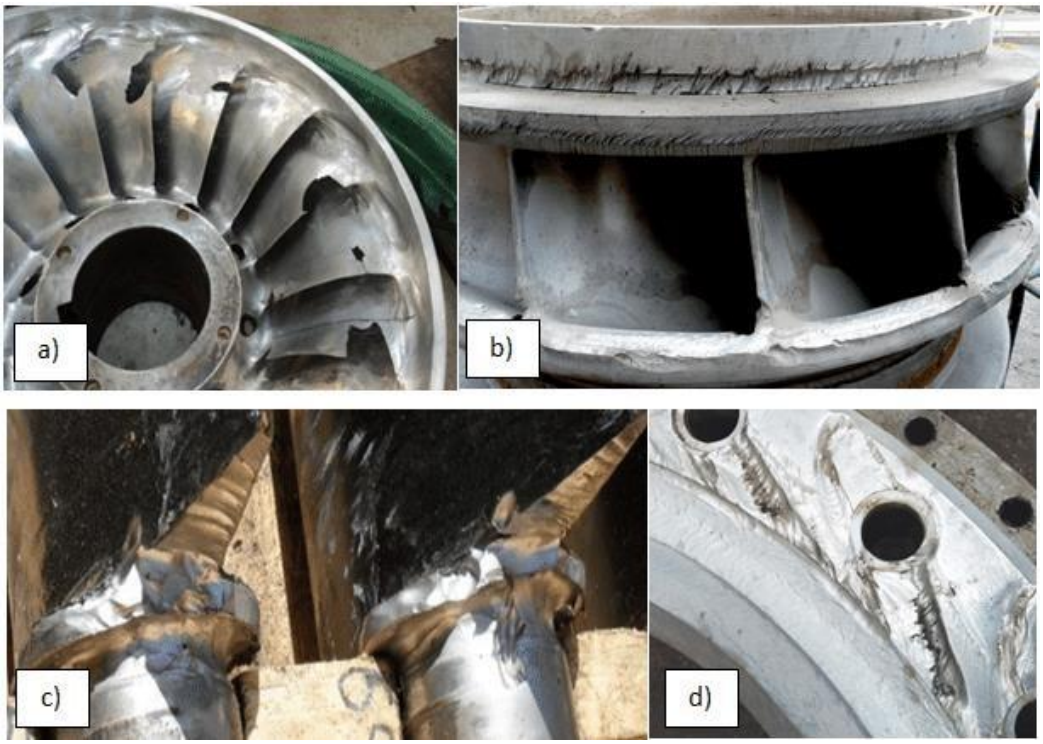

Figure 1. 2 Erosion in Francis turbines at a) Runner outlet, Jhimruk HPP, b) Runner inlet, Cahua HPP, c) Guide vane faces, Middle Marsyangdi HPP, d) Facing plates, Jhimruk HPP (Chitrakar, 2018)

The numerical modeling of flow, is a method that may be used to forecast fluid dynamics properties and performance metrics. It offers a quick and accurate substitute for scale model testing, with simulation modifications carried very rapidly. ANSYS-Fluent software may be used to study the efficiency properties of silt and cavitation erosion using CFD techniques on a hydraulic Francis turbine. Through CFD examination of the runner, guide, and stay vanes, the areas and intensity of erosion can be identified. A numerical erosion model allows for the determination of erosion areas and the degree of intensity.

1.2 Research motivation

The primary renewable energy source for Nepal's rural electrification is hydroelectric facilities. But, after a period of usage, the turbine parts show diminishing performance, mostly as a result of wear and tear, material flaws, silt erosion, and cavitation. This deterioration is attributed to seasonal rivers containing huge amounts of silt with sharp, abrasive particles, such as Quartz. Studying the cavitation phenomenon and sediment erosion effects is essential to reducing damage and enhancing the performance of hydro turbines and their components.

Numerous research initiatives are underway in the Turbine Testing Lab at Kathmandu University, focusing on fluid dynamics to improve hydro turbine performance. However, as of now, there hasn't been a comprehensive study on the interaction between sediment erosion and cavitation in hydroelectric turbines. Exploring this combined phenomenon is critical for extending the lifespan of hydro turbines.

1.3 Objectives

Primary Objective:

- To investigate the combined effects of cavitation and sediment erosion in the Francis turbine.

Specific Objective:

- To investigate the sediment erosion effect in Francis turbine.
- To investigate the cavitation phenomenon in Francis turbine.

1.4 Scope

- Only the impacts of silt erosion and cavitation on runner blades will be predicted by this study.

1.5 Limitation

- The project will not focus on the financial plan for the maintenance of cavitation and sediment erosion effect.
- While performing the simulation, the forms of the quartz particles are solely taken into account as spherical.

CHAPTER 2 LITERATURE REVIEW

2.1 Francis Turbine

The Francis turbine is categorized as an inward reaction turbine with mixed flow. In this design, pressurized water travels radially toward the center after entering the turbine through the guiding vanes and leaving the turbine axially.

Water is conveyed to the turbine and directed to a series of stationary orifices positioned around the runner's circumference. These fixed orifices, also known as guide vanes or wicket gates, play a vital part in controlling the rate of water. The water is guided by stay vanes in the direction of the guidance vanes, where they control the flow and send it in a radial pattern to the runner vane. The water, circulating around the runner, then exits axially through the draft tube.

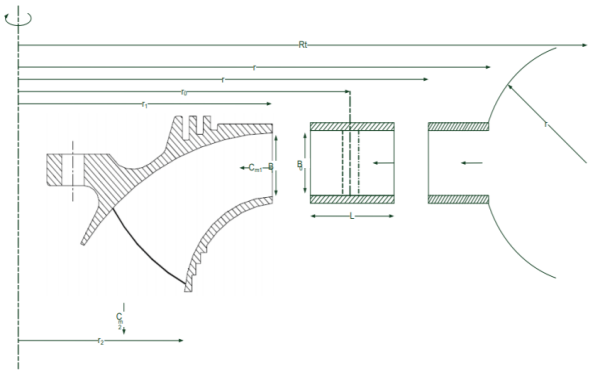

Figure 2. 1 Axial view of Francis turbine (Gjosaeter, 2011)

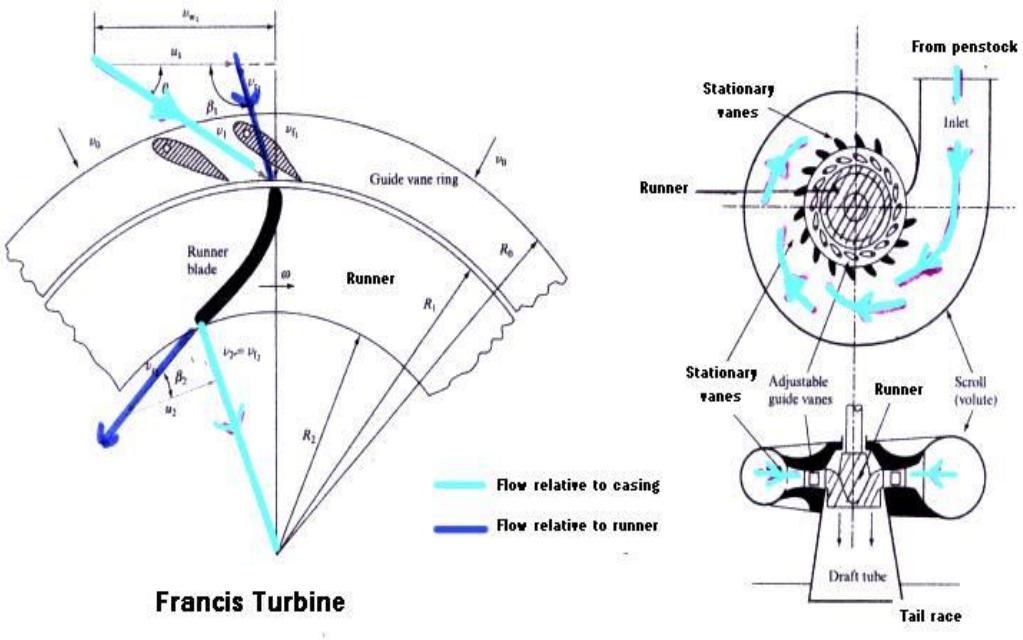

Figure 2. 2 Francis turbine along with its velocity profile (Manandhar, 2019)

2.2 Cavitation

A quick shift in a liquid's pressure can cause tiny, vapor-filled cavities to emerge in places where the pressure is lower than atmospheric pressure. This process is known as cavitation. These cavities are commonly referred to as "bubbles" or "voids." When subjected to increased pressure, these holes produce powerful shock waves. By continuously imploding, the collapse of these voids with the strong shock wave close to a metal surface creates cyclic stress. This process causes the metal's surface to get fatigued, which results in "cavitation," a type of wear.

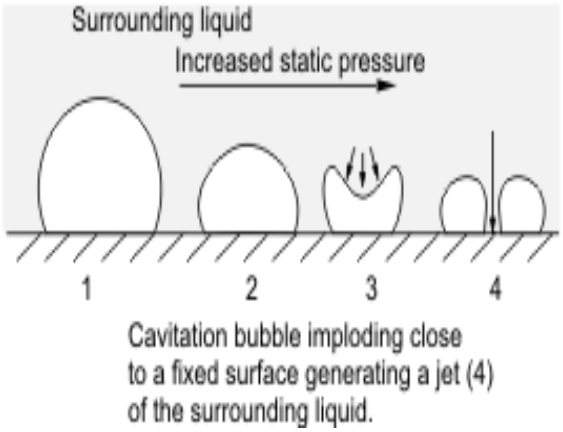

Figure 2. 4 Cavitation phenomenon (Saeed, 2015)

Figure 2. 3 Cavitation damage on runner blade surface (Subramanya, 2013)

Micro-jets develop in the stream flow as a result of cavitation. The impulse from the jet generates pitting on metal parts when these micro-jets strike the casing tip. Turbines that are running under circumstances other than those intended for them, such half load or full load, are more likely to generate larger voids in the flow. (Subramanya, 2013)**.**

In the course of fluid flow through a Francis turbine, the creation and subsequent collapse of bubbles lead to the pitting of metallic surfaces on runner blades or draft tube walls, resulting in noise generation. When a concentration of pits happens in a small space, the material undergoes erosion and mass loss as a result of the repeated cavity collapses.

2.2.1 Types of cavitation

A. Leading Edge cavitation

Leading edge cavitation refers to the phenomenon of cavitation occurring near the leading edge of the blade. Leading edge cavitation in runner blades can occur under certain conditions, particularly when the turbine operates at high speeds or when the flow conditions result in a low-pressure region near the leading edge of the blades. This low-pressure zone can cause the liquid (usually water) to vaporize, forming bubbles. As the water moves downstream along the blade, the pressure increases again, causing the vapor bubbles to collapse.

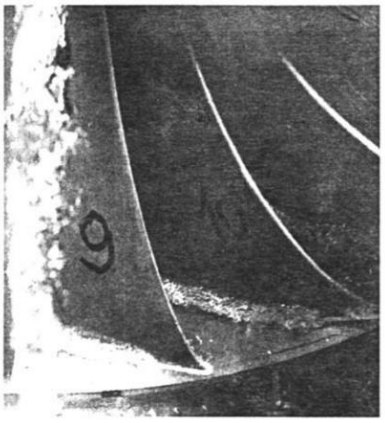

Figure 2. 5 Leading edge cavitation (Saeed, 2015)

B. Travelling Bubble Cavitation

When the local pressure falls below the vapor pressure of the liquid (often water) passing over the blades, traveling bubble cavitation may happen. It appears as divided bubbles in the mid-chord, in close proximity to the trailing edge, and connected to the suction portion of the blade. Low plant cavitation number (σ_p) causes these traveling bubbles to form, which enlarge with increasing load and peak when the machine runs at maximum flow rate under overload circumstances. Numerous things, such as high velocities or poor flow conditions, might cause this. Cavitation bubbles are formed more readily in the low-pressure zones; these bubbles stick to the surface and travel downstream along the blade.

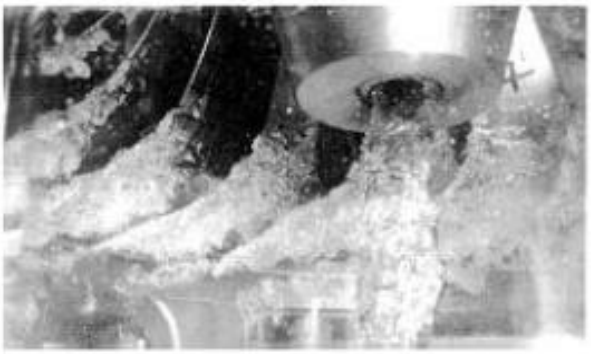

Figure 2. 6 Travelling Bubble Cavitation (Avellan, 2004)

C. Draft Tube Swirl

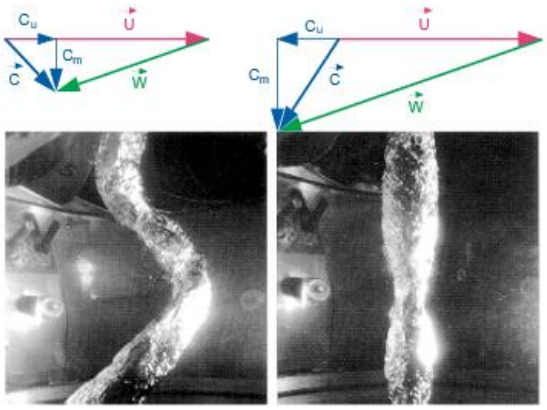

Figure 2. 7 Draft tube swirl (Avellan, 2004)

In a Francis turbine, cavitation resulting from the water's swirling motion in the draft tube is referred to as "draft tube swirl cavitation." It appears at both partial and full load because of the flow's residual circumferential velocity component, which is discharged from the runner. Its volume is dependent on (σ_p). Low-pressure zones may be produced by the water's swirling motion in the draft tube, particularly at specific locations along the walls. Cavitation may happen when the local pressure falls below the water's vapor pressure. In the low-pressure areas, this may cause vapor bubbles to develop.

D. Inter-blade Vortex cavitation

This is created by secondary vortices that arise from flow separation brought on by the change in incidence from the hub to the band and are situated in the channels between the blades. They only cause erosion when their tips make contact with the surface of the runner. When there is a partial load, these vortices form and cause a high amount of wideband noise. Because σ_p is quite low, they can also arise when cavitation happens in highly high-head operation ranges. Here, they become unsteady and produce intense vibrations.

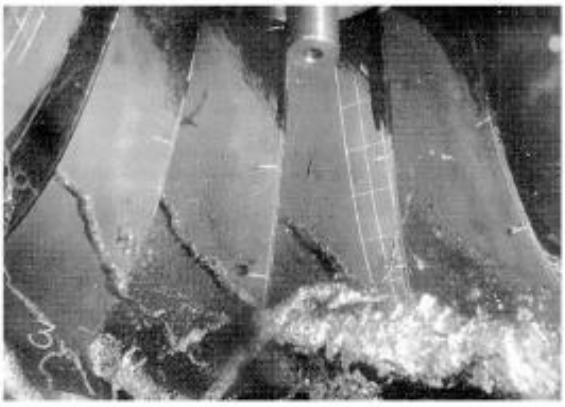

Figure 2. 8 Inter-blade Vortex cavitation (Avellan, 2004)

2.2.2 Thoma's Cavitation Factor

The Thoma cavitation coefficient (σ) is the cavitation number that is used to determine the region in reaction turbines where cavitation occurs. It may be stated as follows;

$$\sigma = \frac{H_a - H_v - H_s}{H}$$

Where, H_a is the head of atmospheric pressure, H_v is the vapor pressure in relation to the water temperature, H_s is the suction pressure at the reaction turbine's outlet, and H is the turbine's operating head.

The parameter σ needs to be greater than the critical cavitation coefficient (σ_c) in order to guarantee the turbine operates without cavitation, a value typically determined during the turbine's design and manufacturing process. While it's challenging to entirely eliminate cavitation, efforts should be made to minimize and keep it inside reasonable bounds. The subsequent empirical connection commonly utilized to determine the value of σ_c. For Francis

$$\sigma_c = 0.625 \times \left(\frac{N_s}{380.78}\right)^2$$

Where, N_s is the turbine's specific speed.

Although the runner design has a major influence on cavitation phenomena, the machine setting level and operating at off-design circumstances are two additional important factors that affect its beginning and development (Chitrakar, 2018).

$\sigma > \sigma_c$, no cavitation condition

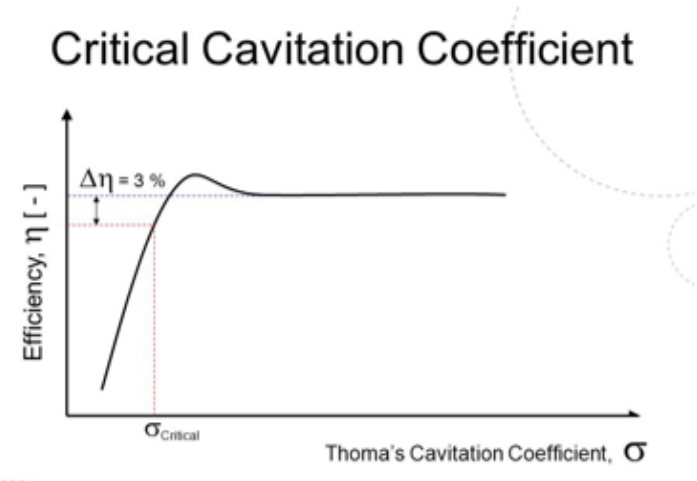

Figure 2. 9 Graph of Efficiency vs Thoma cavitation coefficient (Subramanya, 2013)

2.3 Sediment erosion

The Indian subcontinent alone is home to almost 6 billion tons of the 20 billion tons of materials from Earth that are carried out to sea each year. Similar to other major watersheds that produce sediment, including China's Yellow River (2470 t/km^2/yr), Nepal's Karnali River has an exceptionally high specific sediment output (4363 t/km^2/yr)(Thapa, 2004). The excess sediment in rivers like these is attributed to the severe relief, the existence of unstable rocks, and heavy monsoon rainfall. As a result, sediment management is now crucial for maintaining the longevity, dependability, and safety of infrastructures. It is neither feasible nor cost-effective to remove all fine sediment from water, not even with methods for capturing it. Because of this, the majority of the turbine parts in Himalayan Rivers are subject to water that is heavy with sand, which can cause erosion. The turbine's lifespan and efficiency both decrease as a result of this erosion.

Transport of slit particles in rivers poses a significant challenge for hydropower development, particularly in Himalayan regions like Nepal and other parts of the world. Multiple approaches have been explored to mitigate the effects of silt erosion on runner parts. These strategies include controlling settling basins to screen big particles, trapping sediments at inlets, reducing sedimentation in catchment regions, and protecting turbine parts exposed to high-velocity water with protective coatings. But there hasn't yet been a conclusive answer to this persistent issue in certain regions of the world (Thapa, 2012).

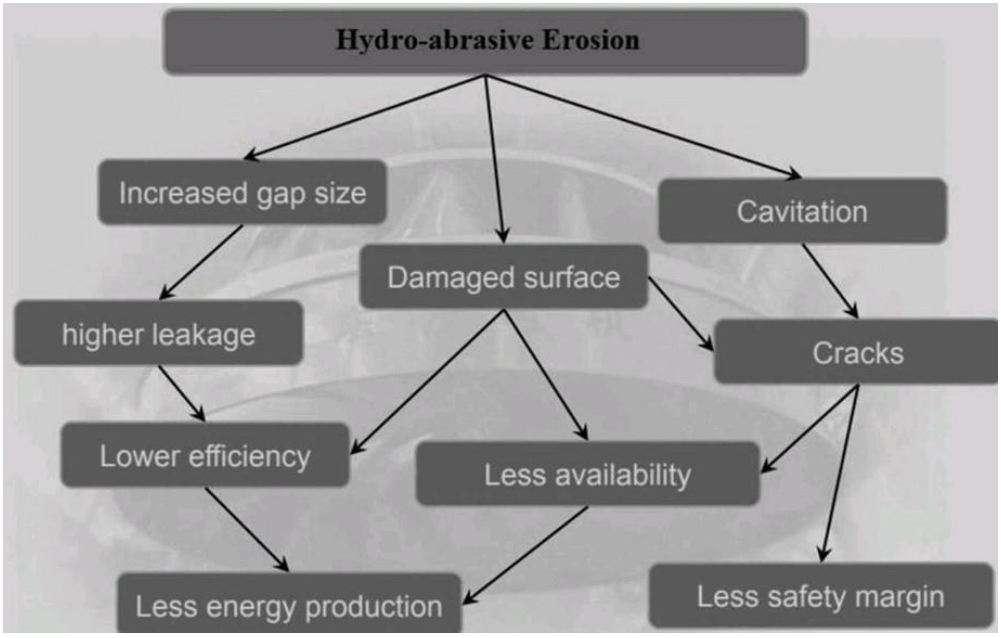

Figure 2. 10 Hydro- abrasive erosion effect in hydro turbines (Sangal, 2018)

2.3.1 Erosion in hydropower projects of Nepal

Nepal's climate and geographical features aggravate the deterioration of turbine parts through sedimentation and eroding. These situations involve high seasonal rainfall, ageing infrastructure, immature geology, technological obsolescence and a tropical climate. Two-thirds of the world's total sediment transported to seas is reportedly attributed to Southeast Asia alone, which makes the problem of erosion even more difficult to solve (Neopane, 2010). In Nepal, sedimentology has become a crucial factor in the majority of new hydropower plants. All of the other projects, including Kulekhani, are run-of-river initiatives that are impacted by sand erosion. Compared to Run-of-River projects, the Khulekhani reservoir project's Pelton turbines experience less erosion since the coarser particles settle before they reach the intake. In Nepalese power plants, fixing the damaged turbines by welding and covering with erosion-resistant hard material is the main tactic against the erosion impact. Figure 2.11 illustrates some of the erosive impacts caused by silt in the Jhimruk Power Plant.

Figure 2. 11 Wear caused by sediment erosion on the Francis turbine's runners and guiding vane in Jhimruk (Thapa, 2015)

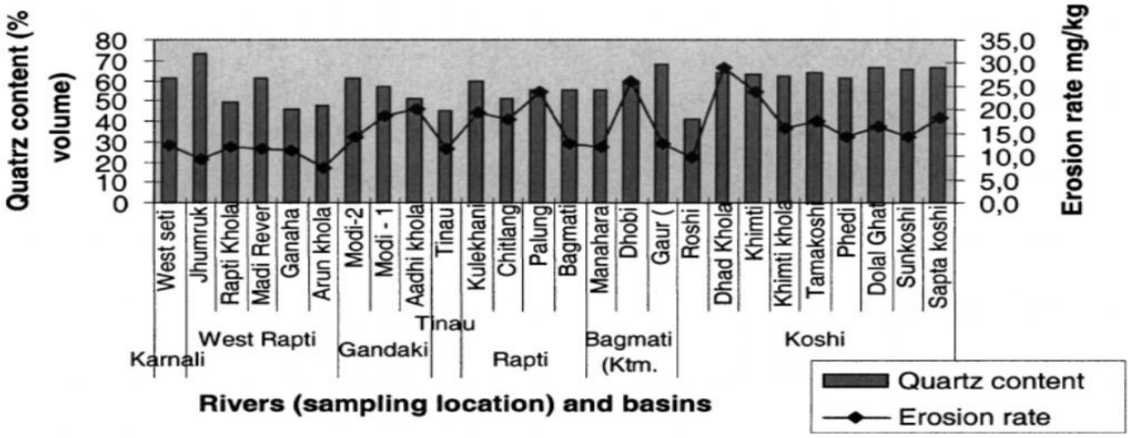

Figure 2. 12 Quartz content from the mineral analysis and the rate of erosion from the laboratory test using the matching sand samples (Neopane, 2010)

2.3.2 Sediment Erosion in Francis turbine

Francis turbines have a speed range of 0.2 to 1.5 in their design. Sediment erosion is the main problem with high-head Francis turbines. With a high-head Francis turbine, the input velocity may reach up to 85–95 m/s, which means that the guide vane faces will experience high absolute velocity and the runner outlet will experience the maximum relative velocity as a consequence. On the other hand, low-head Francis turbines are susceptible to erosion only in the presence of extremely high sediment concentration (Neopane, 2011).

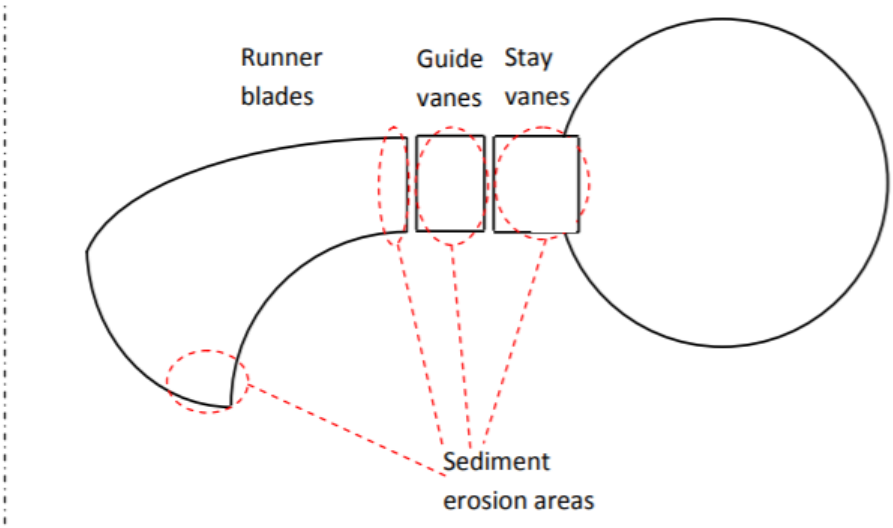

Figure 2. 13 Area exposed to sediment erosion in Francis runner (Gjosaeter, 2011)

Erosion is primarily seen around the runner, stay vanes, and guiding vanes in Francis turbines. The kind of flow phenomena in a given area as well as the operating circumstances determine the amount and pattern of erosion. Francis turbine flow characteristics are quite erratic, particularly in the vicinity of the runner and guide vanes. Predicting the erosion zone would be helpful for creating coating processes and improving hydraulic turbine components, which would solve the issue of erosion in turbine components.

Erosion significantly diminishes performance, alters the flow pattern through the turbine, and can even lead to turbine collapse. Erosion not only poses challenges during maintenance but also diminishes the overall efficiency of the plant. Numerous variables that distinguish between the erosion process and the erosion rate have an impact on erosive wear. Sediment properties, fluid qualities, and base material characteristics are the variables.

2.3.3 Mechanisms of erosion wear

Numerous kinds of wear mechanisms that happen when relatively tiny particles collide with mechanical components are together referred to as "erosion wear". By its very nature, this definition is empirical and has more to do with real-world applications than it does with any deep conceptualization of wear. Figure 2.14 shows the recognized processes of erosive wear.

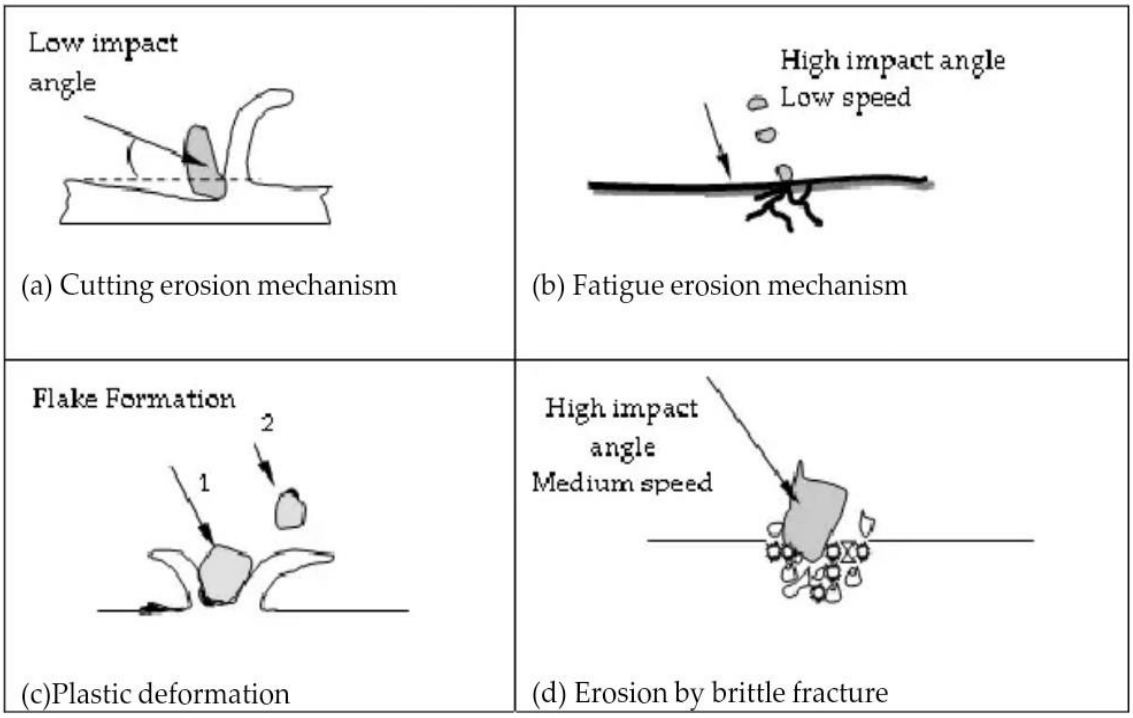

Figure 2. 14 Mechanism of erosive wear (Neopane, 2010)

Cutting erosion:

The erosion process is known as abrasive erosion when cutting is the method used to remove material when there is little impact angle between the particles and the surface. When the abrasive grits come into contact with the surface, they roll or slide, creating an abrasion action that leads to erosion. Short scars the length of a track are left behind when material is removed by the particles' jagged edges with a scraper.

Surface Fatigue:

The process of material deterioration on a component or structure's surface brought on by repetitive pressure, stress, or friction is known as surface fatigue erosion. This kind of erosion is especially prevalent in mechanical systems with cyclic loads on component

parts. Particles that contact the surface at a low speed and with a significant impact angle cause the surface fatigue erosion process. The outermost layer is unable to be plastically distorted; instead, wear and strain causes it to deteriorate, and after many hits, fractures start to appear on the surface. After many hits, the particles will separate from the surface.

Plastic deformation

Particles impacting the elastic surface at a large impact angle and medium speed cause flakes to develop around the striking point, which causes plastic deformation of the surface. The substance will separate into fragments after being struck on the flakes several times.

Brittle fraction

Brittle fracture erosion occurs when medium-velocity particles touch the brittle surface at a significant impact angle. Subsurface cracking causes the sharp particles to separate from the material, increasing the likelihood of brittle fragmentation.

2.3.4 Erosion Rate Expression:

Particle characteristics and paths, local flow and fluctuations fields, surface conditioning, multiphase impacts and the impact of local cavities from material removal are just a few of the variables that affect erosion. The expression for erosion rate is given by:

$$ER = \sum_{p=1}^{N_{particles}} \frac{C_d V^n f(\alpha) m}{A_{face}}$$

Where, m : Particle Mass flow rate

f(α) : Impact angle function

v : Particle impact velocity

n : Velocity exponent

C_d : Particle diameter function

ER : mass of material loss per unit area per unit time [kg/m^2.s]

2.4 Combined effect of cavitation and sediment erosion

The impacts of certain cavitation or erosion processes have been the subject of several theoretical investigations and tests. On the other hand, not much research has been done on how cavitation and erosion work together. In hydraulic laboratories, efforts are being made to tackle this problem from both theoretical and practical angles. The Rotary Disc Apparatus (RDA) is a good test equipment that may be used for this purpose. In high-velocity areas like the runner blades as well as the guiding vanes of a Francis turbine, and the needle of a Pelton turbine, the combined effects of cavitation erosion and sediment erosion may be seen. The intake area of the runner blades, where they connect to the hub and shroud, is one area of the Francis turbine where erosion is brought on by the combined effects of silt erosion and cavitation (Upadhyay, 2007).

Figure 2. 15 Eroded part of Turbine Runner with pure sand erosion and combine effect demarcated (Upadhyay, 2007)

The RDA setup is employed to: (i) create cavitation by adding no sand; (ii) simulate pure sand erosion; and (iii) examine the combined effects of adding cavitation generators and a restricted quantity of sand. Based on the extent and erosion pattern, all three examples are contrasted and examined. The worn-out sections may be visually observed to demonstrate that the combined effect of cavitation erosion and sand erosion is larger than the sum of their separate effects.

2.5 CFD Theory

Within the field of fluid mechanics, computational fluid dynamics (CFD) applies numerical techniques and algorithms to the analysis and resolution of fluid flow-related issues. The conservation of mass, momentum, and energy is the foundation of the basic governing equations of fluid dynamics, upon which CFD modeling is built. CFD uses software tools to describe fluid flow dynamics mathematically and help anticipate fluid behavior. These days, the industry accepts it as a legitimate technical tool that is frequently used. The examination of fluid flow is done through a number of processes in the CFD simulation process. Three phases make up CFD analysis: pre-processing, solver, and post-processing.

2.5.1 Cavitation models

Cavitation models in ANSYS Fluent

ANSYS Fluent offers three different cavitation models:

Singhal et al. Model

Known by another name, the Full Cavitation Model, it can be applied with or without slip velocities to the mixed multiphase model. It takes into consideration all first order effects, including non-condensable gases, bubble dynamics, phase changes, and turbulent pressure fluctuations.

Singhal et al. develop an expression of the net phase change rate using a combination of pair of phase continuity equations;

Liquid phase:

$$\frac{\partial[(1-\alpha)\rho l]}{\partial t} + \nabla.\left[(1-\alpha)\rho l\vec{V}\right] = -R$$

Vapor phase:

$$\frac{\partial(\alpha\rho_v)}{\partial t} + \nabla.\left(\alpha\rho_v\vec{V}\right) = R$$

Mixture:

$$\frac{\partial}{\partial t}(\rho) + \nabla.\left(\rho\vec{V}\right) = 0$$

Furthermore, significant exchange rates are provided by:

$$R_e = F_{vap} \frac{\max(1.0, \sqrt{k})(1 - f_v - f_g)}{\sigma} \rho_l \rho_v \sqrt{\frac{2}{3} \frac{(P_v - P)}{\rho_e ll}} \; when, P \leq P_v$$

Where, l = liquid phase, ρ = mixture density and the constant F_{vap} = 0.02. The liquid-vapor combination is considered to be compressible in this model. Non-condensable gases and turbulence effects have also been considered.

Zwart-Gerber-Belamri Model

The Eulerian multiphase model and the mixing models can both employ this concept. According to this idea, each bubble in a system will be the same size. Additionally, this model's bulk exchange rates are provided by

When $P \leq P_v$

$$R_e = F_{vap} \frac{3\alpha_{nuc}(1 - \alpha_v)\rho_v}{r_b} \sqrt{\frac{2}{3} \frac{P_v - P}{\rho_l}}$$

Where, r_b = Bubble radius $= 10^{-06} m$

α_{nuc} = nucleation site volume fraction $= 5 \times 10^{-4}$

F_{vap} = evaporation coefficient

ρ_v = Vapor phase density

Schnerr and Sauer Model

This model is the standard one. This concept is also applicable to the Eulerian multiphase model and the mixing model. Schnerr and Sauer use a similar methodology to get the formula for the net mass transfer from liquid to vapor, much as in the Singhal et al. model. The resultant expression is

When $P \leq P_v$

$$R_e = \frac{\rho_v \rho_l}{\rho} \alpha(1-\alpha) \frac{3}{r_b} \sqrt{\frac{2}{3} \frac{(P_v - P)}{\rho_l}}$$

Comparison: It is strongly advised to utilize the Zwart-Gerber-Belamri and Schnerr and Sauer models as their numerical results are strong and converge swiftly. While it is physically comparable to the other two models, the Singhal et al. model is more difficult to apply and quantitatively less stable. Furthermore, all of the turbulence models included in ANSYS Fluent are compatible with the Zwart-Gerber-Belamri and Schnerr and Sauer models. (ANSYS Inc.,2012).

2.5.2 Erosion models

Erosion models in ANSYS Fluent

In ANSYS Fluent erosion modeling can be carried out in three approaches:

First: Single phase erosion

Second: Multiphase erosion

Third: Erosion module

ANSYS Fluent in ANSYS 19.2 now has four industry-accepted erosion correlations in addition to default, providing greater flexibility.

Generic Erosion Model:

Under DPM, general formation

$$ER = \sum_{p=1}^{N_{particles}} \frac{\dot{m}_p C(d_p)\, V^n f(\alpha)}{A_{face}}$$

Where, m_p : Mass flow rate of particles

f(α) : Function of impact angle

v : Impact velocity of particle

n : Exponent of velocity

C(d_p) : Function of particle diameter

ER : quantity of material lost in a unit of time and area [kg/m^2.s]

Finnie erosion model: In the case of ductile materials, this model works well since the erosion's expression changes depending on the impact angle and velocity and it's expression is given by:

$$ER = \dot{m} k V^n f(\alpha) \quad \text{with, } f(\alpha) = \frac{1}{3}\cos^2\alpha \quad \text{if } \alpha > 18 \text{ degree}$$

$$f(\alpha) = \sin(2\alpha) - 3\sin^2\alpha \quad \text{if } \alpha \leq 18 \text{ degree}$$

Oka model: Incorporating the influence of wall material hardness, the model offers a more realistic correlation.

McLaury erosion model: Originally designed to forecast the rate at which solid particles in water erode, the McLaury erosion model has mostly been used to slurry flows (Elyyan, 2017).

For single-phase and multiphase CFD simulations, all of the erosion models listed below are accessible:

- Eulerian-Eulerian
- Eulerian-Granular
- Volume of Fluid (VOF)
- Discrete Phase Model (DPM) (Agrawal, 2012)
- Discrete Element Method (Liu, 2013)

CHAPTER 3 RESEARCH METHODOLOGY

3.1 Conceptual Framework

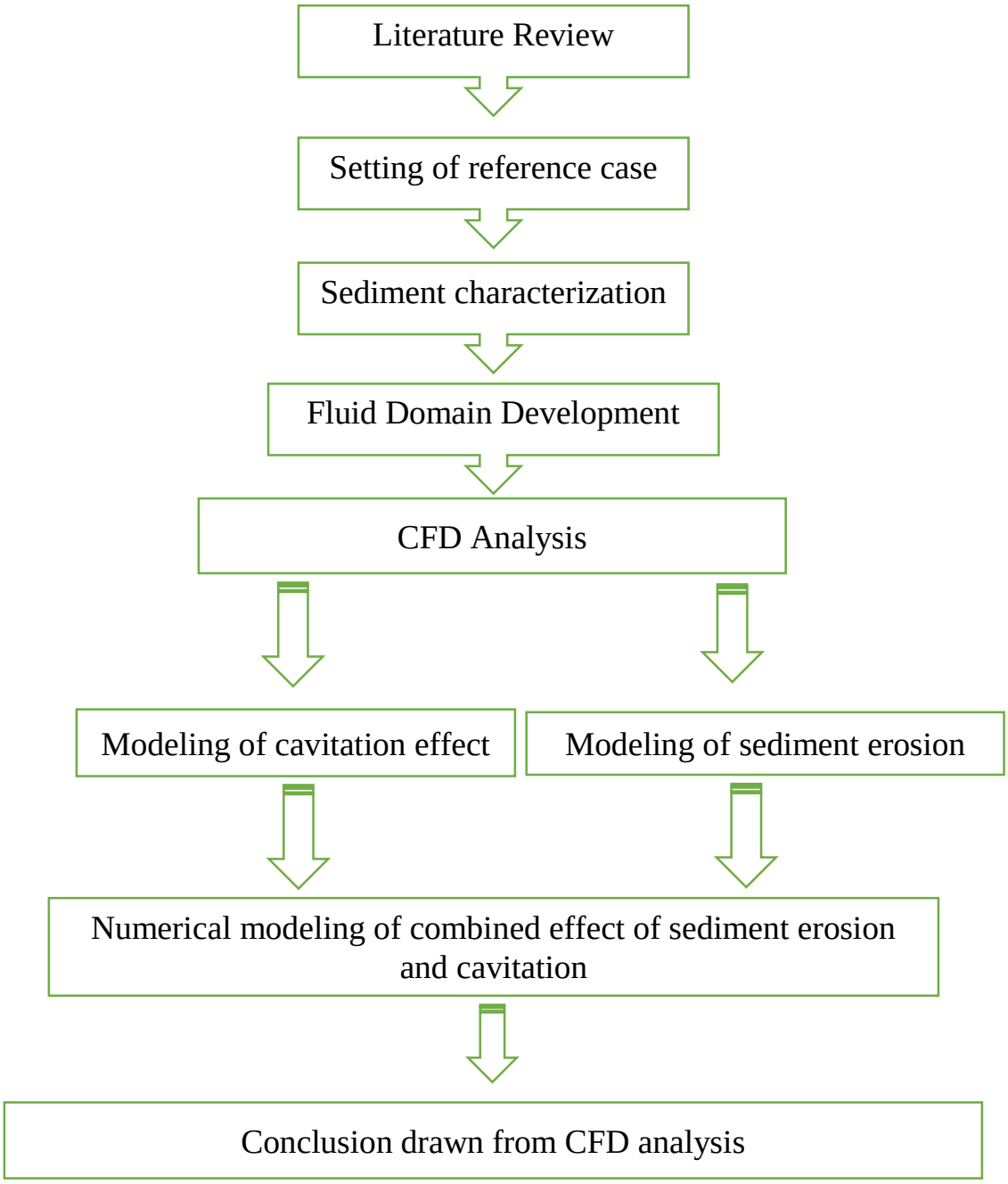

Figure 3. 1 Methodology flow chart

3.2 Setting of reference case

Reference case: **Kali Gandaki "A" Hydroelectric Plant (144MW)**

Key project features:

Type:	Six-hour daily peaking Run-of-River Project
Date of commission:	2002
Reservoir volume:	7.7 Mm^3
Hydraulic Head:	115m (377 ft)
Turbines:	3*48 MW Francis-type
Installed capacity:	144 MW
Spillway type:	Radial gated
Annual generation:	860GWh

In 2002, the Kali Gandaki project commenced its operations. The concrete gravity dam was built to allow for about 3.5 Mm^3 of storage capacity for power peaking. It was designed with radial crest gates for sluicing mode. Figure 3.2 illustrates the general plan of the project's headworks. The intake structure was constructed as an overspill weir, aimed at minimizing sediment entrainment during sluicing, as depicted in Figure 3.3. In the sluicing phase, a desanding basin comes into operation. During big flood occurrences (> 2000 m^3/s), the power plant is temporarily shut down and the dam gates are reopened to allow the water to pass through the reservoir at its full speed.

Operational mode:

During the summer monsoon season, the reservoir operates in sluicing mode when the inflow exceeds twice the design power capacity. In this scenario, the reservoir management prioritizes the controlled release of water to manage the increased inflow. This strategy helps prevent potential overflow and ensures that the reservoir operates within its design limits. However, during the winter season, when the inflow is less than or equal to twice the design power, the reservoir switches to impounding mode. In this mode, the focus shifts to storing water for power generation while maintaining a balance with the inflow. Additionally, when the inflow surpasses 2000 m^3/s, signaling a potential flood risk, the system enters a protective mode. Power production is halted, and the

spillway gates are opened to release excess water and mitigate the flood risk. This proactive approach aims to safeguard the integrity of the reservoir and surrounding areas during periods of heightened inflow.

Major problems:

Sediment-related problems provide two major concerns for the Kali Gandaki hydropower facility. First, there is excessive turbine abrasion at the plant, which weakens the turbine blades. Sand erosion and cavitation together are the main causes of this abrasion. The efficiency and longevity of the turbine components are impacted by wear and tear caused by the abrasive action of sand particles combined with forces generated by cavitation. Second, as coarse material gradually builds up, the reservoir's higher reaches experience increasing flood levels. The water levels rise during flood episodes as a result of this silt accumulation throughout time. The gradual build-up of coarse silt in the reservoir is a problem since it modifies the reservoir's capacity and affects the upstream areas' water levels during times of high flow. Maintaining the Kali Gandaki hydropower plant's best performance and safety requires addressing these sediment-related issues.

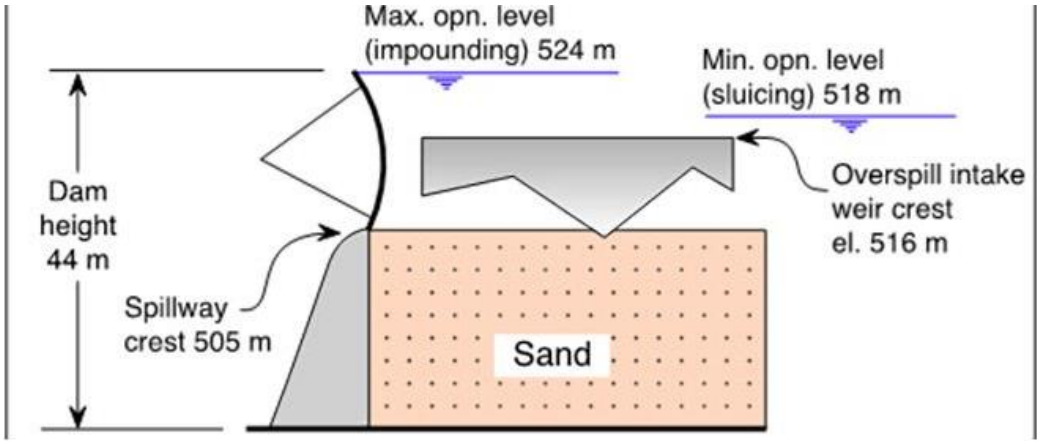

Figure 3. 2 Elevations of the essential hydraulic elements for sluicing sediment (Initiative, n.d.)

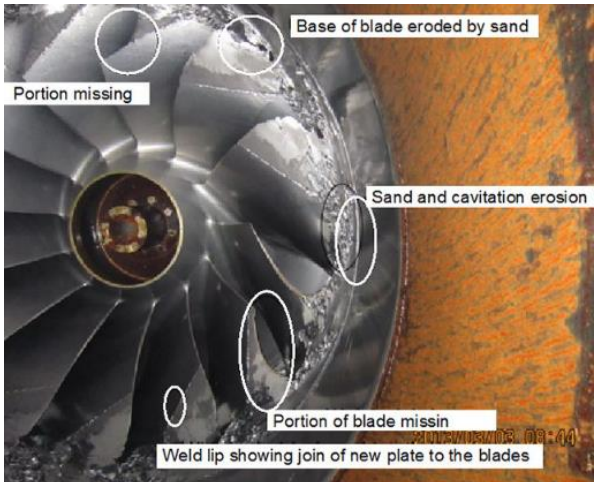

Figure 3. 3 Damage of Francis turbine runner (Initiative, n.d.)

3.3 Sediment characterization

At the dam location, the Kali Gandaki River saw its greatest recorded flood in the previous century, with a flow rate of about 4,500 m^3/s. In contrast, during the dry season, the smallest flow that has been observed is around 40 m^3/s. The amount of sediment that is present varies from 20 parts per million (0.02 kg/m^3) during the dry season to occasionally up to 50,000 parts per million (50 kg/m^3) during the rainy season, which runs from June to September. Figure 3.4 shows that the suspended sand concentration tends to peak in early June and then progressively decline by October of the same year.

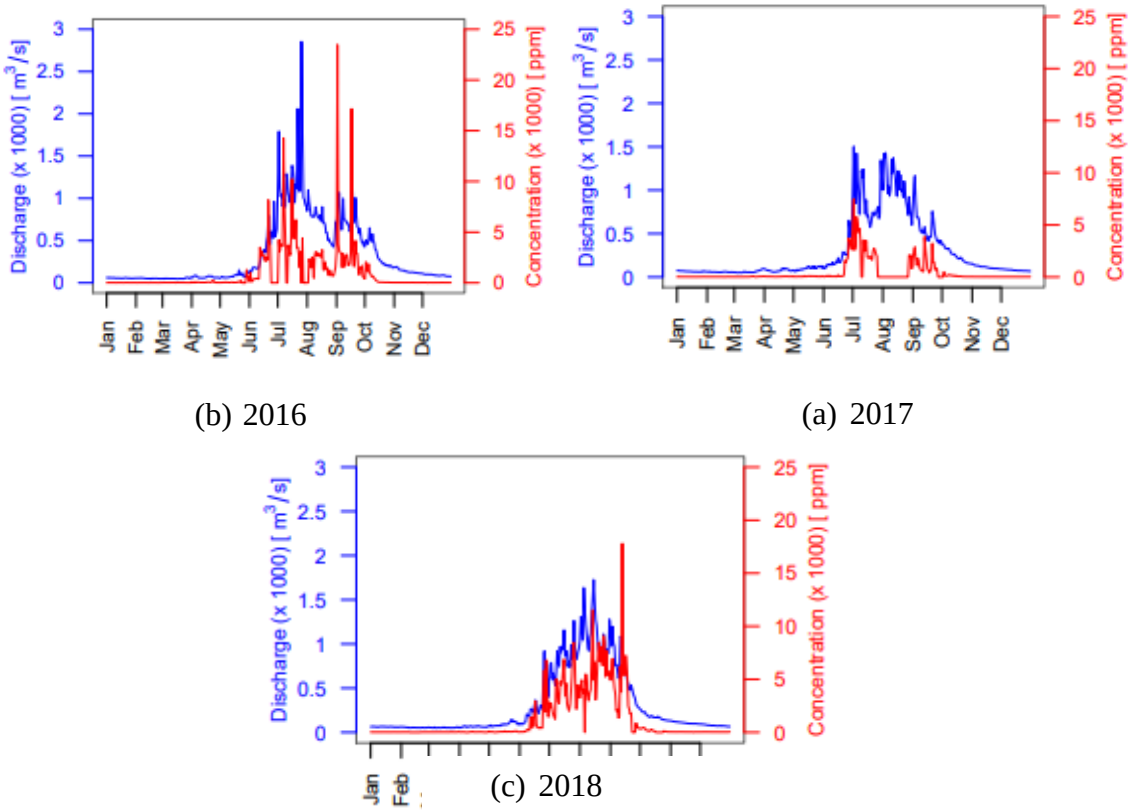

Figure 3. 4 Discharge and sediment concentration for different years of Kali Gandaki river (Shrestha, 2020)

For our case,

Concentration of sediment taken = 6000ppm

We know that,

$$1 \text{ ppm} = \frac{1\,mg}{1\,Kg}$$

$$6000 \text{ ppm} = \frac{6000\,mg}{1\,Kg}$$

$$1 \text{ ppm} = \frac{0.006\ Kg\ of\ sediment}{1\ Kg\ of\ water}$$

At BEP, Water flow rate = 47, 000 Kg/s

Then,

$$\text{Total flow rate of sediment} = \frac{0.006\ Kg\ of\ sediment}{1\ Kg\ of\ water} \times 47{,}000\ Kg/s$$

$$= 282 \text{ Kg/s of sediment}$$

For single passage,

$$\text{Flow rate of sediment} = \frac{Total\ flow\ rate\ of\ sediment}{Number\ of\ blades}$$

$$= \frac{282}{13} = 21.7 \text{ Kg/s}$$

The design of the sediment basin at Kali Gandaki "A" efficiently eliminates any sediments larger than 0.2 mm in size of the particles. Additionally, it effectively blocks around 70% of sediments with a particle size bigger than 0.10 mm and 95% of particles having a grain size larger than 0.15 mm. Given that particles with diameters below 0.1 mm can enter the runner blades, I have opted for a quartz particle diameter of 0.1 mm (Chhetry, 2015).

3.4 CFD Analysis

A subfield of fluid dynamics known as CFD uses numerical techniques and algorithms to solve fluid flow issues. Reducing the amount of time and money needed to forecast model behavior in an actual setting is one of the main benefits of CFD analysis. In this study, the impact of sediment erosion, cavitation, and their combined effects on the blades of a reference case Francis turbine is investigated using CFD techniques with ANSYS Fluent Software.

3.4.1 Computational model for Francis turbine

A Francis runner with thirteen blades makes up the computational geometry for the CFD analysis. The Francis runner's design was provided by the Kathmandu University Turbine Testing Lab, and the shape was created using Bladegen. A right-handed orientation coordinate system was utilized, and the runner's rotational motion was centered around

the z-axis with a rotational speed of 300 rpm during the design phase. The normal layer thickness of the blade shape design is 41 mm at the leading edge, gradually decreasing to 14 mm at the trailing edge. Figures 3.5 and 3.6 display the runner's blade thickness and angle progression, respectively, as adopted in the design.

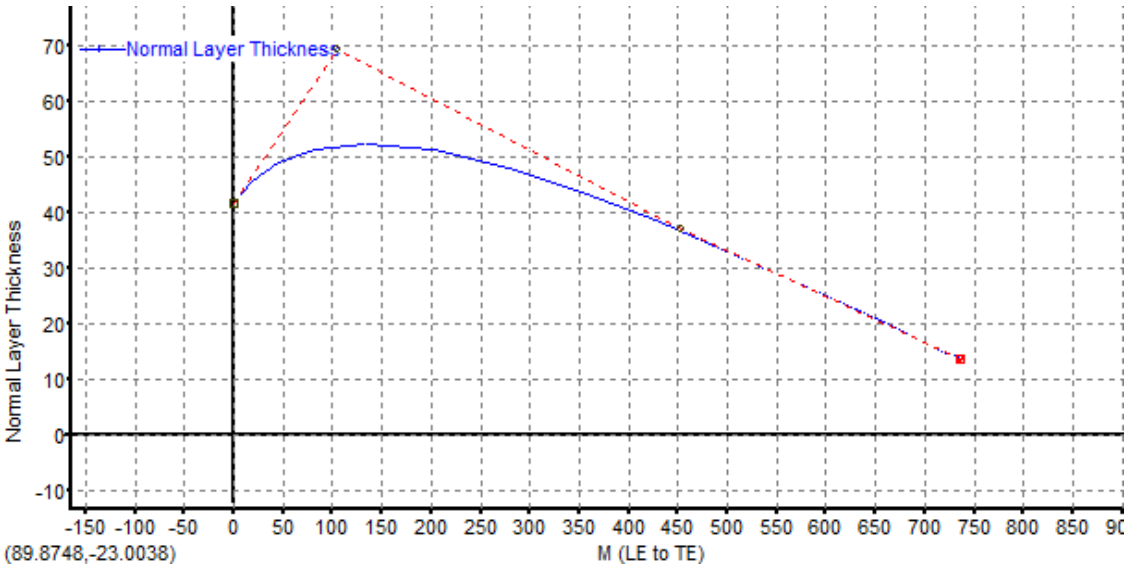

Figure 3. 5 Blade thickness progression

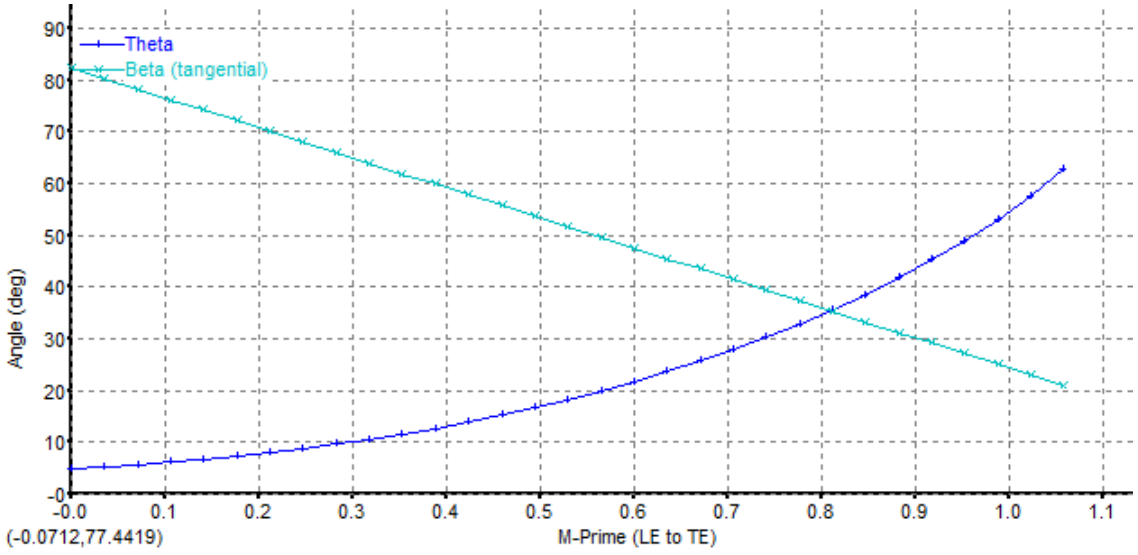

Figure 3. 6 Blade angle progression

3.4.2 Mesh Generation

Ansys TurboGrid Release 19.2's Automatic Topology and Meshing (ATM optimized) tool was used to construct the mesh for the Francis Runner. This equipment is renowned for its capacity to produce fine meshes with little manual labor. The runner blade domain, initially constructed in the BladeGen blade modeler, is then imported into ANSYS TurboGrid to create a high-quality hexahedral mesh. This mesh is developed after specifying the blade profiles, hub, shroud faces, and fluid domain.

The y^+ variables define the mesh resolution. As can be clearly seen in Figure 3.7, the y^+ value represents the non-dimensional distance between the wall and the first mesh node.

Numerically y^+ value is defined as

$$y^+ = \frac{\rho \times \Delta y \times u_\tau}{\mu}$$

where, $u_\tau = \left(\frac{\tau_\omega}{\rho}\right)^{(1/2)}$ is the friction velocity and Δy is the separation between the first mesh node and the wall., τ_ω is the wall shear stress, ρ is the density of fluid and μ is the dynamic viscosity.

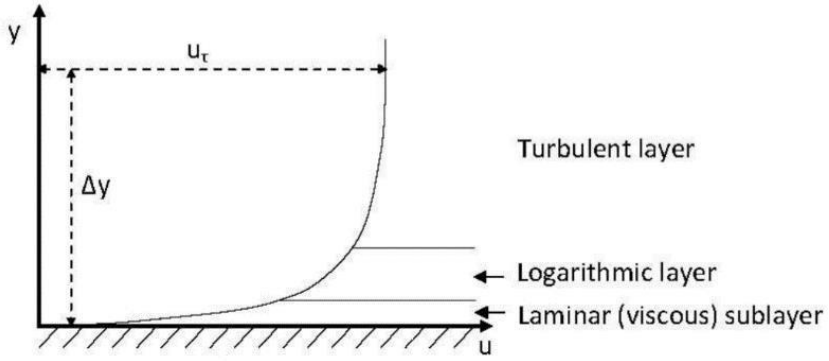

Figure 3. 7 Wall Function (Thapa, 2011)

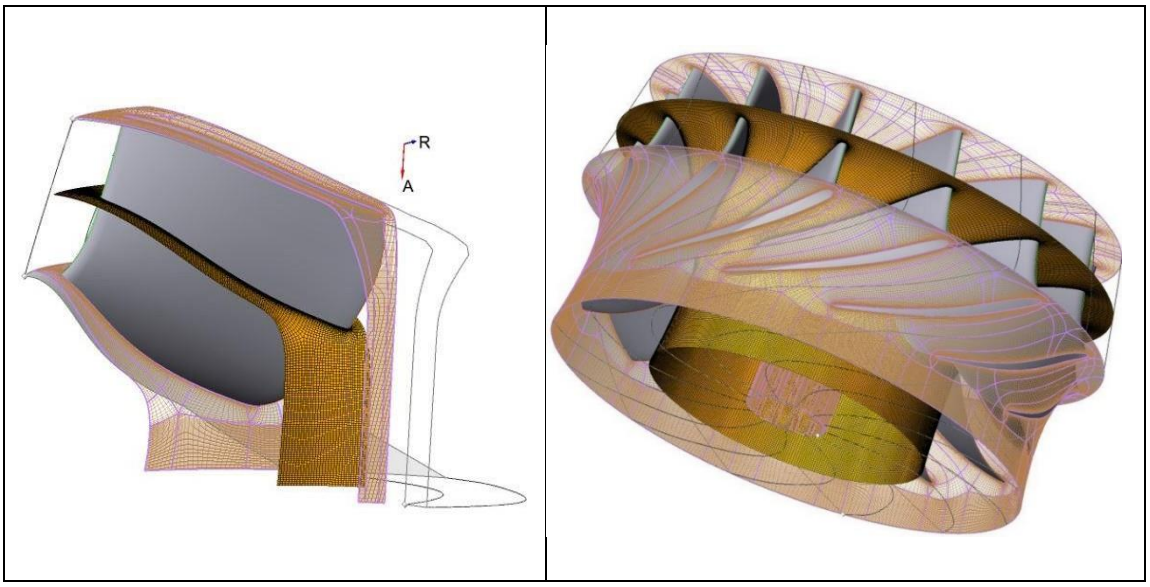

Figure 3. 8 Mesh generation in ANSYS Turbogrid 19.2 (left-single blade view; right- full runner)

Turbulence modeling, boundary conditions and Fluent setup:

The Francis runner's single blade was the subject of the simulation. The boundary types for the blade, hub, and shroud were defined as moving walls, with their motion relative to the adjacent cell zone, representing the fluid passage. The motion of these parts followed a rotational pattern about the Z-axis. Boundary walls were considered non-slip and smooth. The SST k-omega turbulence model was used to address the turbulence in the fluid. The simulation focused on the BEP of the turbine, achieved when the guide vane angle was set to 20 degrees, and the corresponding flow rate of water was 47,000 kg/s. considering that the runner blade was analyzed within a single passage, the mass flow rate at BEP was calculated as 3615.38 kg/s. The inlet flow direction was specified using cylindrical coordinates, namely (a, r, t), where the values were set as (0, -0.34, -0.93). The runner had chosen to rotate at a speed of -300 revolutions per minute.

Mesh independence study:

In the mesh convergence study, we initiated with a size factor of 0.5 and a factor ratio of 0.5 to achieve rapid solution convergence. This study focused on monitoring parameters such as torque, head, and y-plus values. When the factor ratio was set to 1, the head appeared to converge quickly (in under 150,000 nodes). However, an issue arise with the runner's torque, which exhibited instability, with a decreasing trend as the number of nodes increased. This behavior may be attributed to elevated y-plus values, which failed to adequately capture the viscous sub-layer. To address this concern, we systematically increased the size factor and factor ratio in an iterative manner. The head and torque values seemed to stabilize after reaching approximately 600,000 nodes, with changes of less than 1 percent even as the node count was raised to 3 million. The plot of mesh convergence behavior is shown in figure 3.9. From figure 3.9 (a) and (b) it can be concluded that around 6 lakh nodes is enough to obtain fully mesh independent solution.

Finally at the end we chose the mesh having 6, 06, 431 nodes and 5, 76, 280 elements with y plus value 6.90 on the runner blade for further simulation.

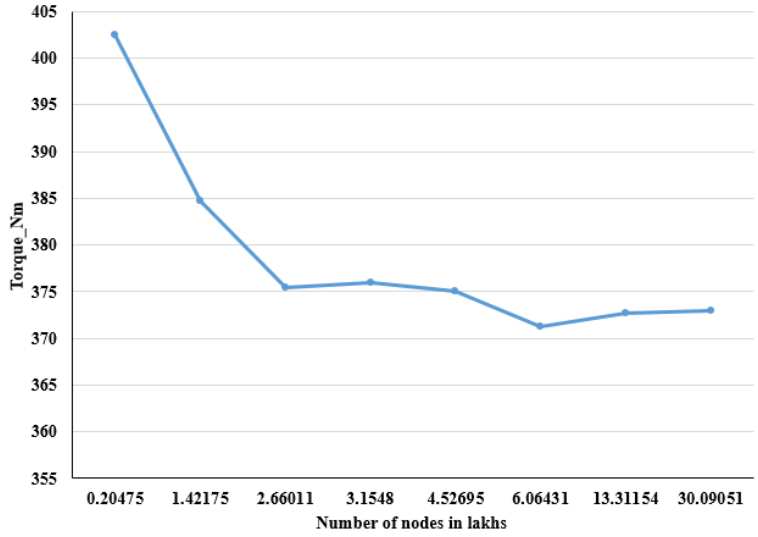

(a)

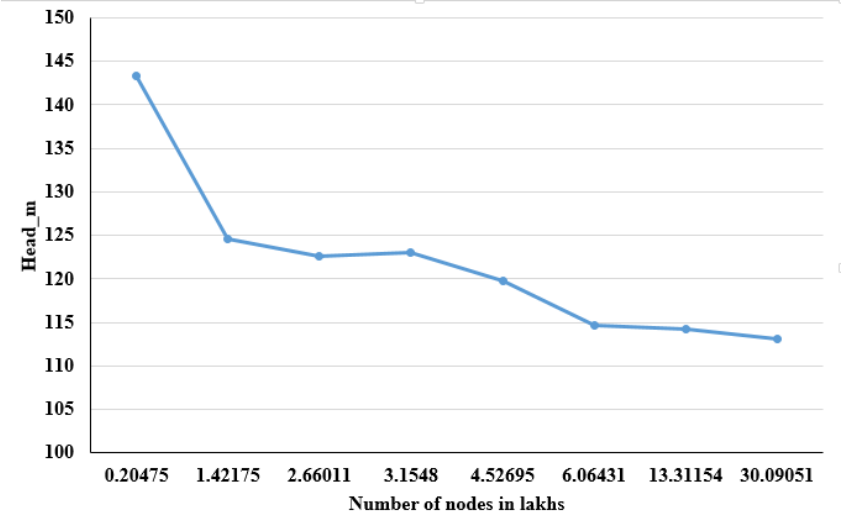

(b)

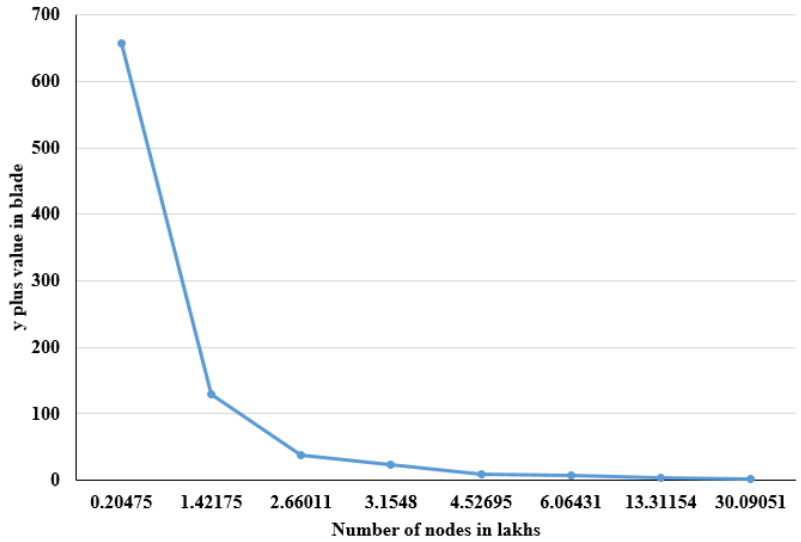

(c)

Figure 3. 9 (a) & (b) Mesh independence study with varying size factor & factor ration; (c) y plus dependency on node count

3.4.3 Cavitation analysis in ANSYS Fluent

Model used:

The Schnerr and Sauer Model, which serves as the default model within the mixture multiphase model, was employed in this simulation. There were two separate phases identified: the liquid phase, which is the major phase, and the vapor phase, which is the secondary phase. The Schnerr and Sauer models are known for their robustness and quick convergence, making them a highly recommended choice. The SST k-omega turbulence model was used to address the turbulence in the fluid.

With a combination of water and vapor that contains a large number of spherical vapor mixtures, the cavitation model is carried via the interface between the liquid and vapor phases to mass transfer, representing the processes of evaporation and condensation, respectively(Zheng, 2018).

$$R_e = \frac{\rho_v \rho_l \alpha_v (1-\alpha_v)}{\rho_m} \frac{3}{R_B} \sqrt{\frac{2(p_v - p)}{3\rho_l}}$$

$$R_c = -\frac{\rho_v \rho_l \alpha_v (1-\alpha_v)}{\rho_m} \frac{3}{R_B} \sqrt{\frac{2(p - p_v)}{3\rho_l}}$$

where α_v is proportion of local vapor void, ρ_m is phase density in mixture and ρ_v is phase density of vapor.

Table 3. 1 Domain parts defined as per required boundary type

S.N	Domain Parts	Boundary type
1	Inflow	Mass-flow Inlet
2	blade	Wall
3	hub	Wall
4	Shroud	Wall
5	Outflow	Pressure outlet

Boundary Condition

The Francis runner's single blade was the subject of the simulation. The boundary conditions were set according to the naming given to the different parts of the domain. Different domain was defined as shown in table 3.1.

Moving walls are the boundary kinds for the blade, hub, and shroud. These components continue to move in relation to the fluid channel, or nearby cell zone. The motion is set as rotational about the Z-axis. The Multiphase Mixture model is employed to simulate the steady-state water-vapor flow in the Francis runner, utilizing two Eulerian phases for water and vapor to induce cavitation effects. Boundary walls were considered non-slip and smooth. The SST k-omega turbulence model is employed to address the turbulence phenomena of the fluid. The simulation is conducted at the BEP of the runner, which is achieved when the guide vane angle is 20 degrees and the corresponding flow rate of water is 47,000 kg/s. Since the runner blade is analyzed in a single passage, the mass flow rate at BEP is 3615.38 kg/s. Cylindrical coordinates are used at the entrance to specify the flow direction that is; (a, r, t): (0, -0.34, -0.93). The runner had chosen to rotate at a speed of -300 revolutions per minute.

3.4.4 Sediment erosion analysis in ANSYS Fluent

Model used:

- Dense Discrete Phase model (DDPM) was activated to study the effect of sediment erosion. DDPM approaches Lagrangian way to flow the quartz particle in the defined domain.
- All four default erosion correlations were activated while performing the simulation i.e. Generic, Finnie, Oka and McLaury erosion models.
- The fluid's turbulence phenomena was explained using the SST k-omega turbulence model. Because it benefits from the strengths of the k-epsilon model in the free stream and the Wilcox model close to the wall, the SST k-omega model was chosen.

Defining Sediment injection Properties:

After configuring the models, the sediment injection properties must be set up. The sediment is designated as quartz, and the injection type is chosen as surface. Since the quartz particle needs to be injected from the inflow surface, inflow is selected. The particle, in this case, is inert in nature, and its material is specified as anthracite by adjusting its density to 2650 kg/m^3. In the point properties section, the diameter of sediment particles is set at 0.0001 m, representing the average size of sediment particles found in the Kaligandaki River. The selected sediment concentration is 6000 ppm. At the Best Efficiency Point (20 deg. Guide vane angle), the flow rate is determined to be 47,000 kg/s, and the overall sediment particle flow rate is set at 21.7 kg/s.

Boundary Condition

The Francis runner's single blade was the subject of the simulation. The boundary types for the blade, hub, and shroud were defined as moving walls, with motion relative to the adjacent cell zone, representing the fluid passage, and rotational about the Z-axis. The inflow boundary type was set as mass-inflow inlet, while the outlet was designated as pressure-outflow outlet. For the Discrete Phase Model (DPM) settings, the DPM boundary condition type, erosion models, and particle tracking restitution coefficients were configured. The DPM boundary condition was set as "reflect type" for walls (blade, hub, and shroud), and "escape type" was selected for both the inlet and outlet. The Takeoff and Grant Rebound Erosion model coefficients were incorporated under the Discrete Phase Reflection Coefficients settings. Both the normal and tangential

directions of sediment impact were considered, and the coefficients from the Tabakoff and Grant Rebound Erosion Model were applied to all three parts: blade, hub, and shroud. The impact angle, which depends on the imperfections, toughness, and sharpness of the pipe surface, determines the restitution coefficient in most cases. Because of energy transfer, the particle's reflected velocity is lower than its entering velocity upon collision. The coefficient of restitution depending on momentum describes this impact signature. The restitution coefficient for sand-steel, used in this case, is illustrated in Figure 3.10.

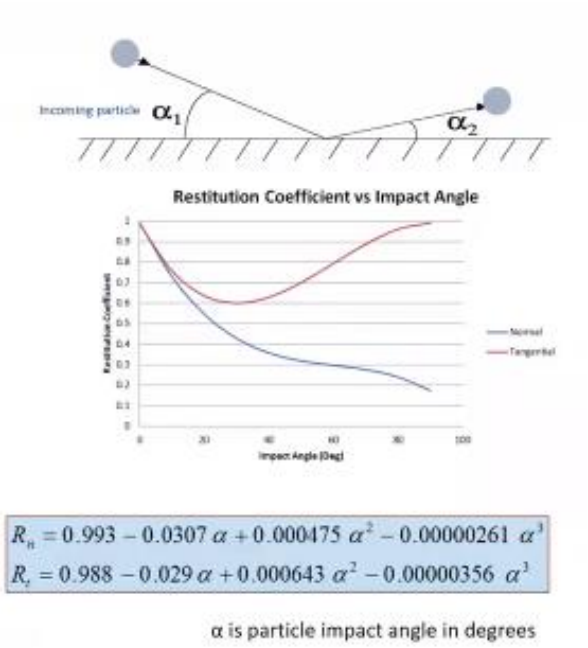

*Figure 3. 10 **S**ample Restitution coefficient for sand-steel*

The inflow boundary type was configured as a mass-inflow inlet. The simulation is conducted at the BEP of the turbine, which is achieved when the guide vane angle is 20 degrees, and the corresponding flow rate of water is 47,000 kg/s. However, since the runner blade is analyzed in a single passage, the mass flow rate at BEP is 3615.38 kg/s. Cylindrical coordinates are used at the entrance to specify the flow direction that is; (a, r, t): (0, -0.34, -0.93). The runner had chosen to rotate at a speed of -300 revolutions per minute.

Erosion with different operating condition:

To explore the impact of different operating conditions, specifically part-load and full-load scenarios, a series of simulations were conducted. These simulations involved varying guide vane angles, mass flow rates, and sediment inflow rates. The guide vane angle was adjusted within the range of 10º to 30º, while the mass flow rate for a single passage was varied from 1807.69 Kg/s to 5423.08 Kg/s, and the sediment inflow rate ranged from 10.85 Kg/s to 32.55 Kg/s. Table 3.2 provides a comprehensive overview of all the varied parameters, which were adjusted in relation to the BEP parameter, with BEP serving as the reference point at 100 percent.

Table 3. 2 Varied parameters for part load and full load conditions

	Alpha angle	Radial component	Tangential comp.	Sediment flow rate, kg/s	Q in 1blade, Kg/m^3	Net pressure head, Pa	Efficiency, %
Part Load	10	0.174	0.985	10.85	1807.69	127.0049623	96.01
	11	0.191	0.982	11.94	1988.46	127.9915209	96.06
	12	0.208	0.978	13.02	2169.23	127.2945178	96.78
	13	0.225	0.974	14.11	2350.00	127.2598889	97.02
	14	0.242	0.970	15.19	2530.77	127.0151845	97.12
	15	0.259	0.966	16.28	2711.54	127.3511957	97.30
	16	0.276	0.961	17.36	2892.31	127.1903252	97.40
	17	0.292	0.956	18.45	3073.08	127.1791030	96.80
	18	0.309	0.951	19.53	3253.85	127.1424546	97.37
	19	0.326	0.946	20.62	3434.62	127.6201988	97.40
BEP	20	0.342	0.940	21.70	3615.38	127.2348909	97.53
Full Load	21	0.358	0.934	22.79	3796.15	127.0256478	96.86
	22	0.375	0.927	23.87	3976.92	127.3218897	96.62
	23	0.391	0.921	24.96	5423.08	127.2508430	96.38
	24	0.407	0.914	26.04	4338.46	127.3638950	96.12
	25	0.423	0.906	27.13	4519.23	127.6225525	95.84
	26	0.438	0.899	28.21	4700.00	127.5586524	95.55
	27	0.454	0.891	29.30	4880.77	127.6306075	95.26
	28	0.469	0.883	30.38	5061.54	127.3386932	94.98
	29	0.485	0.875	31.47	5242.31	127.6546157	94.67
	30	0.500	0.866	32.55	5423.08	127.1910928	94.37

3.4.5 Combined effect analysis in ANSYS Fluent

Background of ANSYS Fluent

Multiphase model:

A phase in multiphase flow is characterized as a distinct class of material having a specific inertial response to and interaction with the potential field submerged in the flow.

Eulerian model:

Out of all the multiphase models in ANSYS FLUENT, the Eulerian model is the most intricate. For every phase, it resolves a set of continuity and momentum equations. The interphase exchange coefficients and pressure work together to create coupling. The kind of phases involved determines how this coupling is handled specifically; non-granular (fluid-fluid) flows are handled differently from granular (fluid-solid) flows.

Dense Discrete phase model:

With ANSYS FLUENT, one may solve the transport equations for the continuous phase and simulate a discrete second phase inside a Lagrangian frame of reference. The spherical particles that make up this second phase are scattered throughout the continuous phase. Using this model, quartz particles have been injected, allowing for the investigation of erosion's impact on Francis runners.

Lagrangian and Eulerian Approach

When analyzing fluid flow using the Lagrangian technique, it is assumed that the fluid is made up of a very large number of particles, each of which needs to have its motion defined. On the other hand, the Eulerian method describes the properties of a flow field as a function of space coordinates and time, employing control volume analysis. It is essential to remember that the Lagrangian technique is used to analyze the effects of sediment erosion, while the Eulerian approach is used to investigate the impact of water vapor on the runner profile, specifically the cavitation effect.

Due to the advantage of ANSYS Fluent, which is able to study both the approaches i.e. Lagrangian and Eulerian approach simultaneously we used ANSYS Fluent to study the correlation between cavitation and sediment erosion in Francis runner.

Numerical approach:

Eulerian-Lagrangian (E-L) approach is used to simulate the steady state water-vapor-sediment flow in Francis runner. To activate E-L approach Multiphase Eulerian-Dense Discrete phase model was used.

Number of Eulerian phases: By employing the Multiphase Eulerian method, two phases i.e. water and vapor were assumed to be a mixture of fluid, which was simulated by solving the continuity and momentum equation.

Number of Dense Discrete phase model (DDPM): One i.e. quartz particle.

Boundary Details: Simulation was performed for only one blade of the Francis runner. Cylindrical coordinates are used at the entrance to specify the flow direction that is; (a, r, t): (0, -0.34, -0.93). The runner had chosen to rotate at a speed of -300 revolutions per minute. Multiphase Eulerian-DDPM was used to simulate the steady state water-vapor-sediment flow in Francis runner. There were two number of Eulerian phases i.e. water and vapor which able us to induce the cavitation effect whereas single particle phase used under DDPM to inject the quartz particle at in-passage inflow surface to induce erosion in Francis runner. Boundary walls were considered non-slip and smooth. The fluid's turbulence phenomena was explained using the SST k-omega turbulence model. Consistent, incompressible, homogeneous flow was supposed to be the flow condition. The particle and size composition of the river sediments varies, containing clay (<0.002 mm), silt (0.002-0.030 mm), sand (0.06-2.00 mm), gravel (2-60 mm), and other materials. The specific gravity of the sediments is around 2.65. Quartz was thus selected for the particles. A molar mass of 68.08 kg/kmol is utilized, and quartz has a density of 2650 kg/m^3. A value of 0.1 mm is the mean diameter of the particles. For DPM settings, the DPM boundary condition type, the erosion models and particle tracking: restitution coefficients were setup. The DPM boundary condition was kept “reflect type” for walls i.e. blade, hub and shroud whereas for inlet and outlet “escape type” was selected. The Takeoff and Grant Rebound Erosion model coefficients were included under the Discrete Phase Reflection Coefficients settings. The flow rate of water was set to 3615.38 kg/s for all simulations in this study, while the flow rate of sediment was set to 21.7 kg/s. The static pressure at the outflow was adjusted to one atmosphere.

CHAPTER 4 RESULTS AND DISCUSSION

4.1 Cavitation result:

Mass Transfer rate:

Cavitation represents a thermodynamic phase change process, primarily involving mass transfer. This phenomenon entails the mass and volume transfer between the liquid and vapor phases. It encompasses both the collapse (condensation) and the creation of bubbles (evaporation). These factors are considered when identifying the regions prone to cavitation on the blade. It's important to note that a rise in the condensation rate results in a more concentrated condensation, which in turn contributes to the predictably more severe occurrence of cavitation.

1. **Pressure Distribution over Runner**

Figure 4.1 shows the distribution of pressure throughout the runner under half load, rated load, and full load conditions. It is evident that the pressure gradually drops from the casing entrance to the runner's exist due to the energy extraction process, while the velocity follows the expected characteristics of a reaction turbine, increasing from the entrance to the exist of the runner. Furthermore, the suction side of the runner blade exhibits low-pressure zones, which cause vapor bubbles to develop there, as illustrated in Figure 4.1 and 4.2. The full load condition exhibits significantly lower pressure levels throughout the runner when compared to the half load and rated load conditions. This results in a heightened cavitation effect and reduced efficiency during full-load operation.

2. **Volume Fraction of Water Vapor**

The vapor parameter's volume fraction was used to predict the cavitation region on runner blade. The fractional amount has a range of 0 to 1, where 1 represents 100% of the vapor bubbles. Figure 4.2 shows the distribution of water vapor volume over the runner blade under part load, rated load, and full load conditions, respectively. It is evident that the suction side of the blade experiences higher vapor bubble formation, which indicates that here is where cavitation effects are prevalent. It is also found that effect of cavitation is found highest at the full load condition as compare to BEP and part load condition.

Part Load

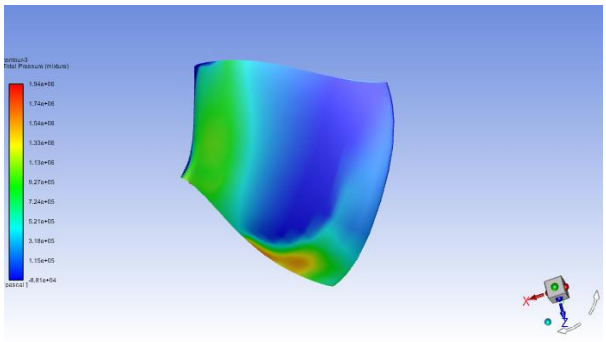

Suction side

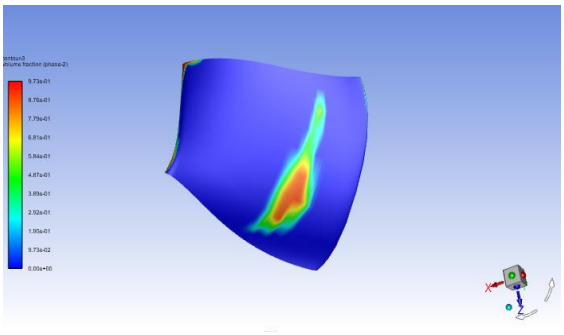

Suction side

BEP

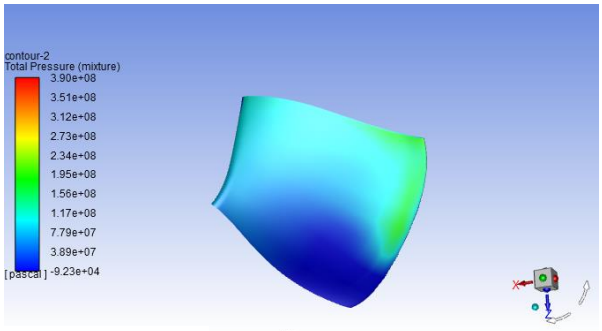

Suction side

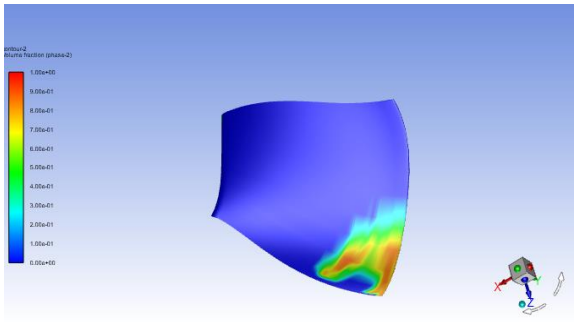

Suction side

Full Load

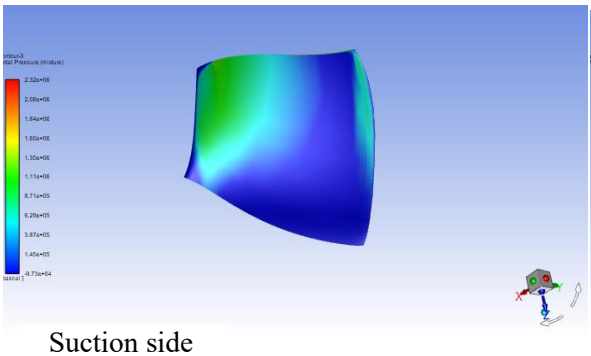

Suction side

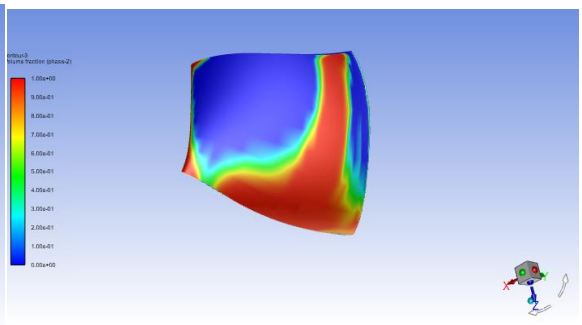

Suction side

Figure 4. 1 Pressure distribution on runner at part load, rated load and full load condition

Figure 4. 2 Vapor volume fraction on the runner at part load, rated load and full load condition

4.2 Sediment erosion result

Erosion rate density

Simulation findings are used to create contour plots of erosion rate density on the Francis turbine's runner blade. An effective way to measure erosion is to look at the erosion rate density (kg/m^2s) parameter, which relates to flow-induced pressure and shear stress. A post- processor takes the predicted erosion data. The contour plots of projected erosion rates are generated using this post-processor. This allows to identify areas with a high of erosion. Colored dots can be observed as a result. The color red represents the maximum erosion intensity value, while the color blue represents the lowest erosion intensity value.

Figures 4.4, 4.5, and 4.6 depict the erosion predictions on the runner blade surface under part load, rated load, and full load conditions, respectively. The most significant erosion is anticipated at the trailing edge on the pressure side of the blade surface, as higher relative velocity occurs in these regions of the runner. The elevated relative velocity leads to increased particle movement, resulting in a more pronounced erosion effect in these areas. Additionally, erosion is observed at the leading edge of the suction side.

Part Load

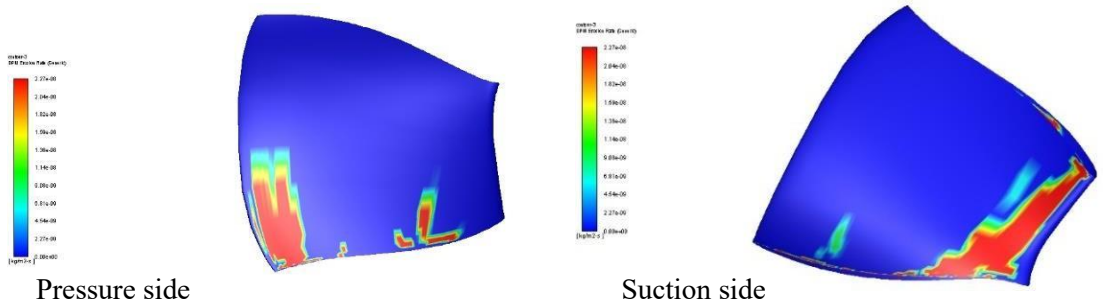

Figure 4. 3 Erosion in the pressure and suction side of the blade at part load

BEP

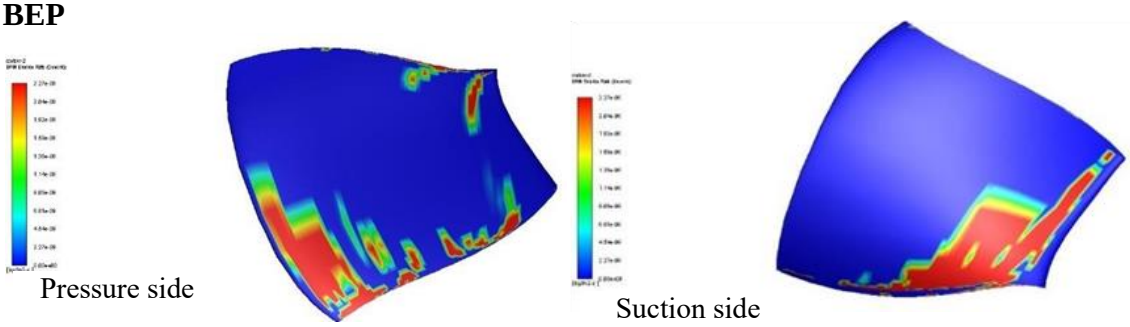

Figure 4. 4 Erosion in the pressure and suction side of the blade at BEP

Full Load

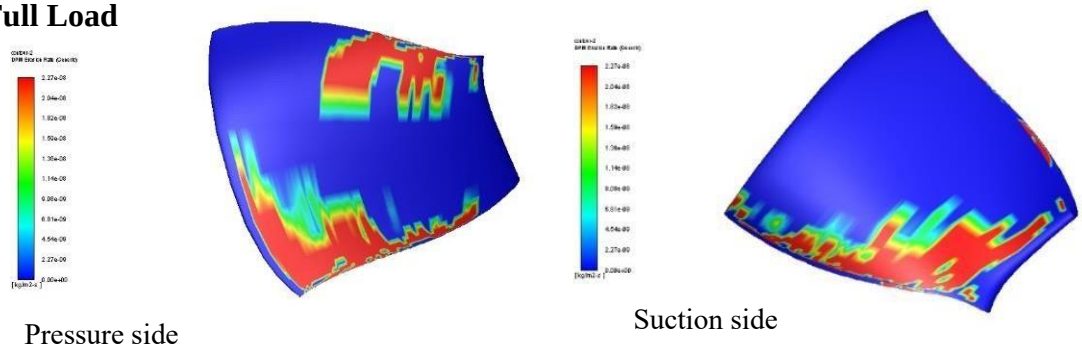

Figure 4. 5 Erosion in the pressure and suction side of the blade at full load

Effect of operating condition in erosion:

To investigate the effect, there were simulations run with varying guide vane angles, flow rates of water and sediment were guide vane angle varied from 10º to 30º, mass flow rate from 1807.69 Kg/s to 5423.08 Kg/s and sediment inflow rate from 10.85 Kg/s to 32.55 Kg/s. Based upon the simulation results obtained, effects of operating condition on erosion rate density on the turbine blade along pressure side is shown in figure 4.6, as is obviously clear that erosion rate density is high as we increase the guide vane opening angle. The increase in erosion rate density on the blade surface with increase in GV opening, as the velocity is more at the more opening of GV angle. The majority of the particles will go towards the blade surface because to the high velocity, increasing the erosion impact. Together with this I have calculated torque, pressure inflow and pressure outflow value for each case to calculate the efficiency of the runner for different operating condition. The calculate efficiency is shown in table 3.2 and a graph was plotted between efficiency vs varying guide vane angles with different operating condition which is shown in figure 4.7.

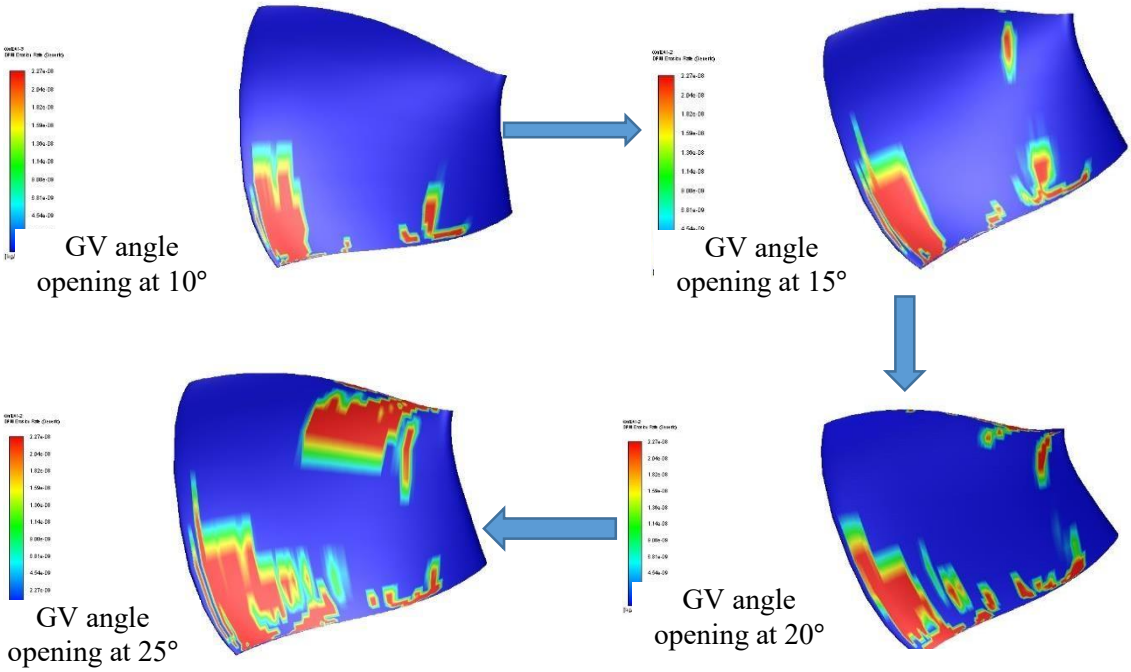

Figure 4. 6 Increase in erosion rate density on the blade surface with increase in GV opening

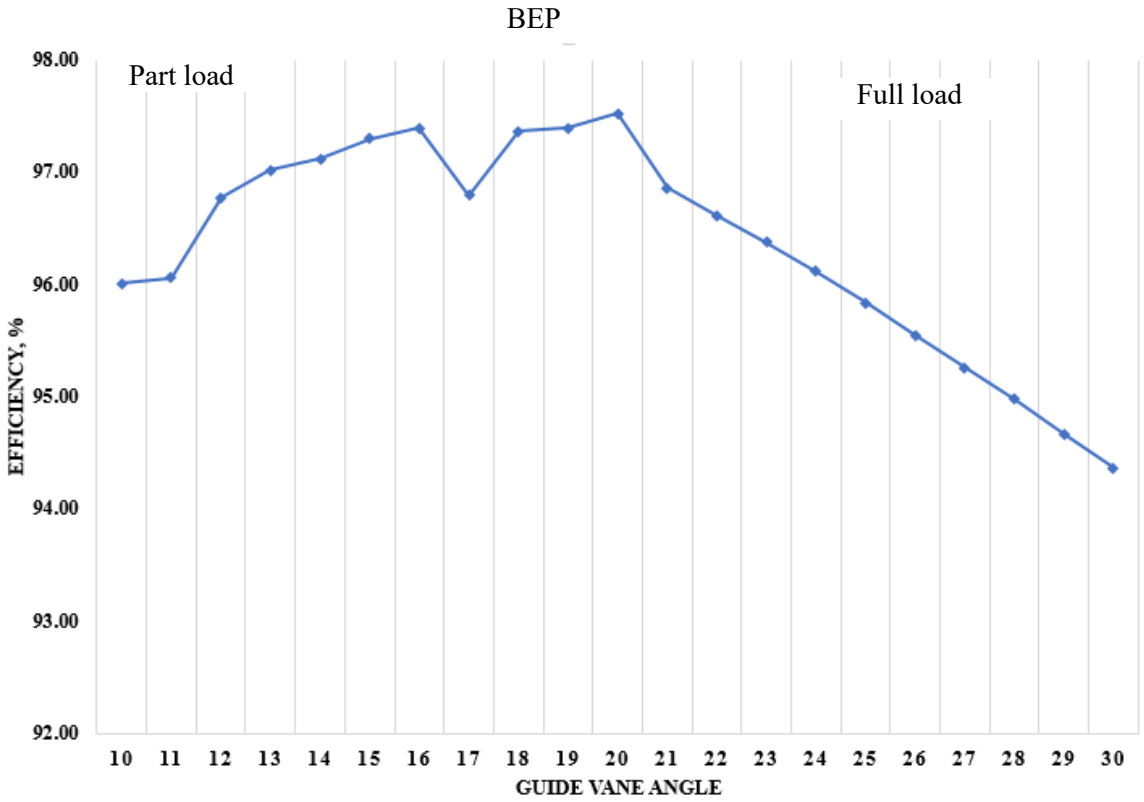

Figure 4. 7 Graph showing the effect of percentage change in efficiency for varied load condition

When I perform simulations under various operating conditions, it also discover that the maximum erosion rate density on runner, 2.27e-08 $kgm^{-2}s^{-1}$, is predicted for the full load condition. Table 4.1 lists the calculated erosion rate densities for different operation conditions.

Table 4. 1 Effect of change in flow rate on erosion rate density along with change in GV angle

Operating Condition	**GV angle (degree)**	**Erosion rate density ($Kgm^{-2}s^{-1}$)**
Part load	14	9.21E-09
BEP	20	1.63E-08
Full load	26	2.27E-08

4.3 Combined effect obtained using ANSYS Fluent

1) Mass transfer rate

In case of cavitation effect only in ANSYS Fluent water transported the air bubbles towards the high-pressure zones area; but, in the event of a combined action, vapor bubbles were transported into the high-pressure area by both water and well slit. Cavitation is hence more severe under combined erosion working conditions. For only cavitation phenomenon, vapor volume fraction is found maximum at suction side of trailing edge of the runner blade, but when we introduce the sediment particle along with the vapor bubble on the setup, the effects seen on the trailing edge increases.

Figure 4.8 illustrates the mass transfer over blades of the runner with the Multiphase Eulerian Dense Discrete phase model in ANSYS Fluent. Figure 4.8 illustrates how the pressure and suction sides of the blades are affected in addition to the runner blade's trailing edge. The pressure side was not affected when only vapor bubbles were introduced to the setup.

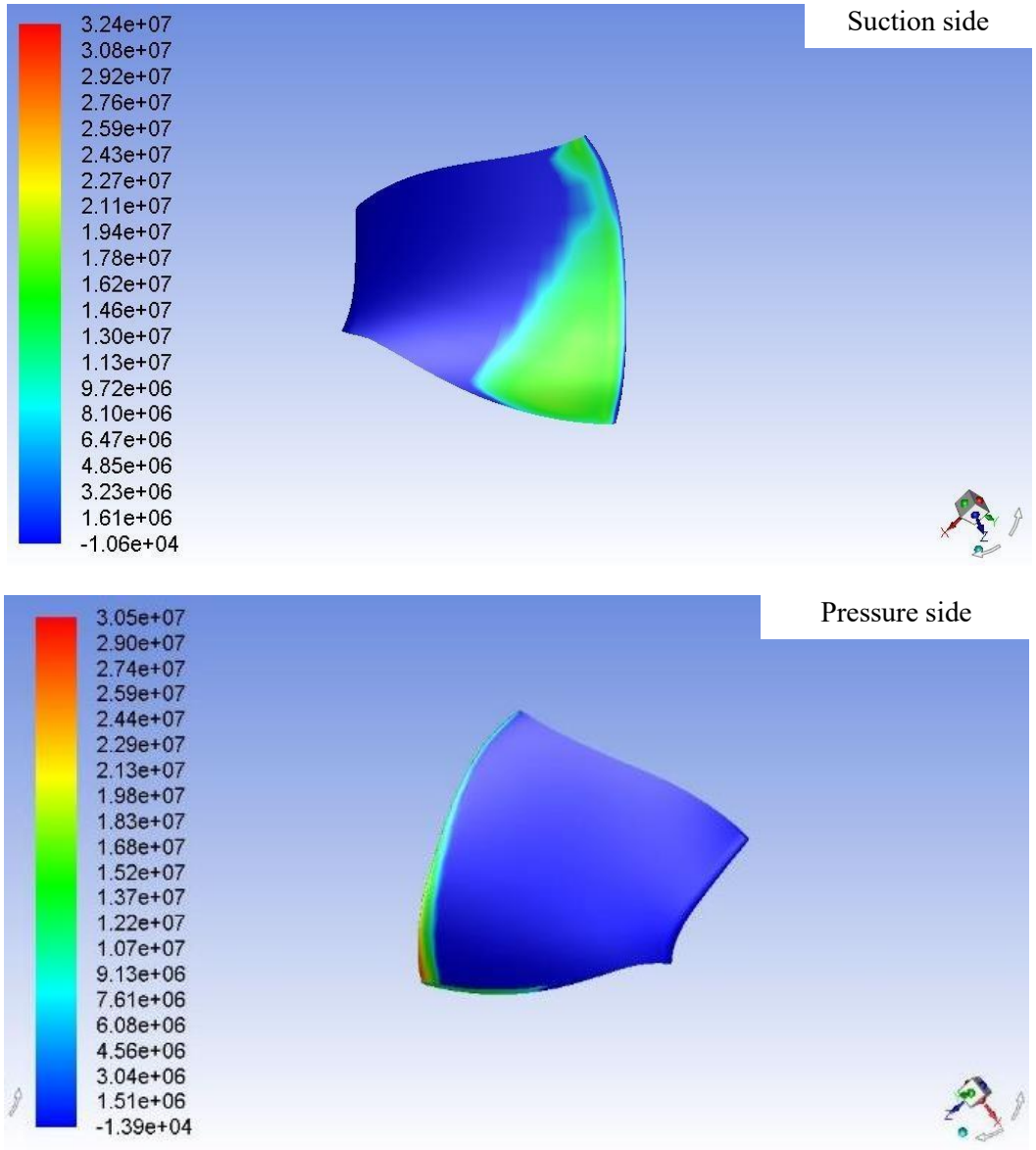

Figure 4. 8 Cavitation effect during the combined effect

2) Erosion rate density

When the ANSYS Fluent simulation was used just to investigate the impact of quartz particles in runner blades, erosion was seen at the trailing edge on the pressure side of the runner's blade surface because these areas of the runner had higher relative velocities. But when I used Multiphase Eulerian DDPM in ANSYS Fluent to determine the combined effect of sediment particles and vapor bubbles, the effect was shown to be more severe.

Figure 4.9 shows the eroded areas over blade profiles of Francis runner using Finnie model in ANSYS Fluent. The pressure side of trailing edge is greatly affected which is caused because of the combined impact of sediment particles and vapor bubbles. It also discover that the erosion rate density on runner, 7.52e-05 $kgm^{-2}s^{-1}$, is predicted for combined condition which is 4.61×10^{3} times greater than the erosion rate density obtained while studying the effect of sediment erosion effect only at BEP.

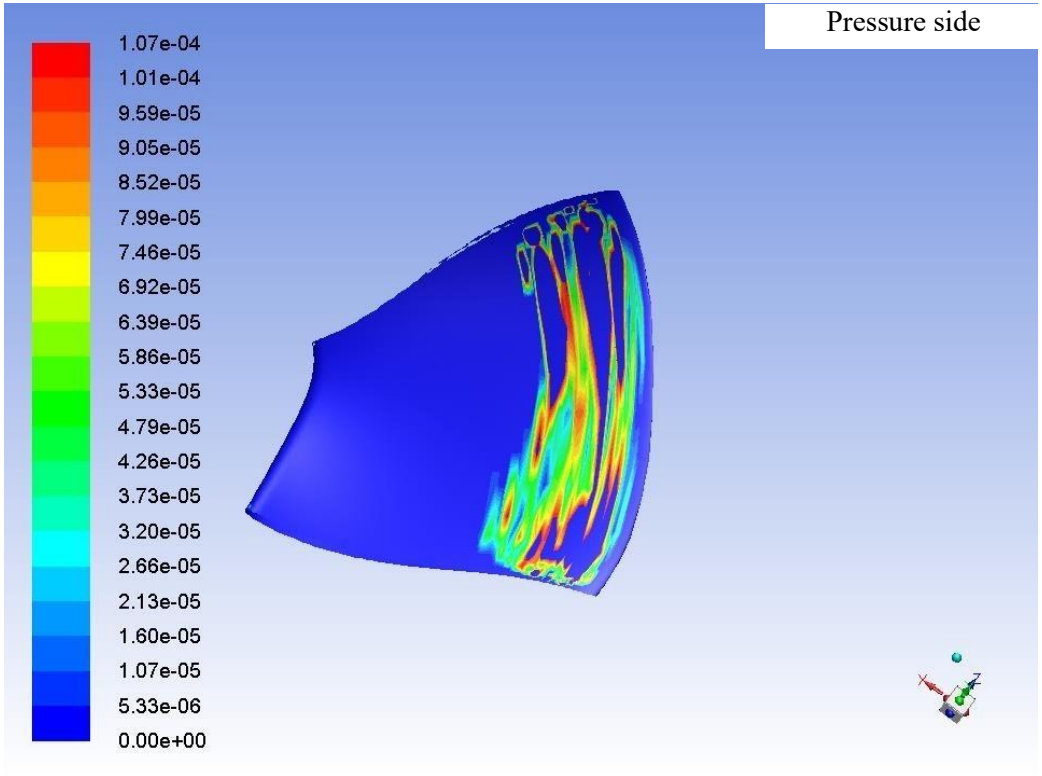

Figure 4. 9 Erosion rate density during the combined effect

CHAPTER 5 RESULT COMPARISON

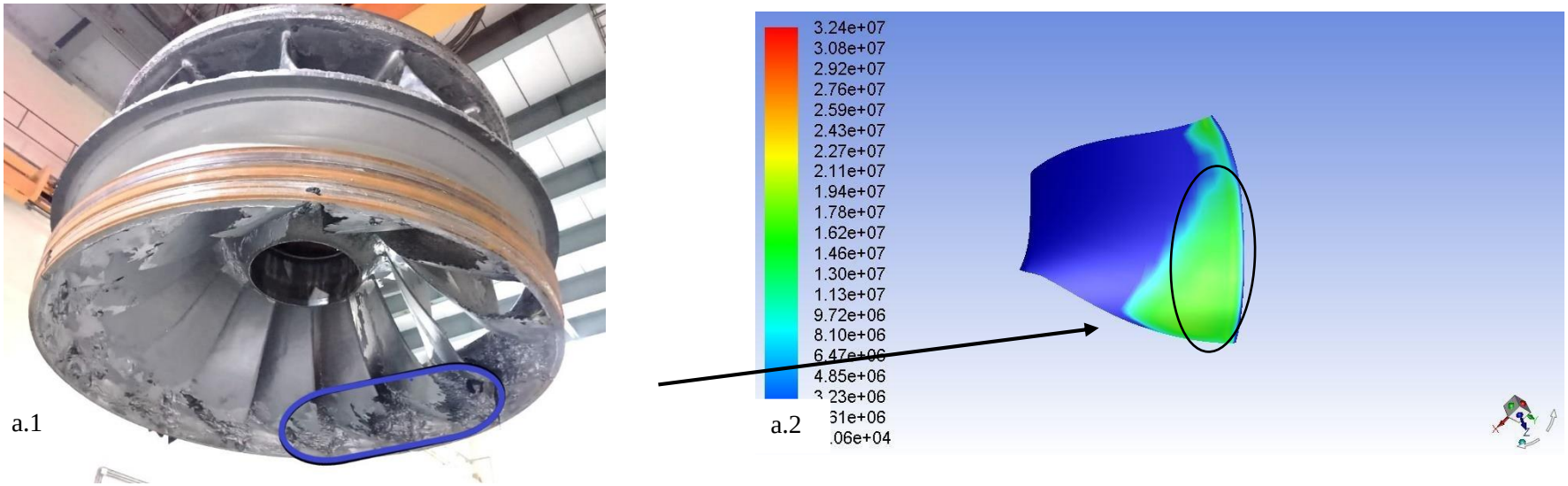

Figure 5. 1 Comparison of the mass transfer obtained from ANSYS Fluent with the actually affected/eroded model

Figure 5.1 (a.1) shows the extensive damage caused by sediment-water-vapor at discharge of a Francis runner of Kali Gandaki "A" Hydroelectric Plant (144MW) **(Cr: Mr Binod Pandey, an NEA Engineer)**; here the combined effect has penetrated the blades. Similar pattern of damage were observed when we performed the simulation in ANSYS Fluent Multiphase Eulerian DDP model. The area that is highly affected by the cavitation was predicated using mass transfer rate in the combined effect and was noticed maximum at suction side of trailing edge of the blade profile. The area marked by the circle in the figure 5.1 (a.2) indicates the location of the cavitation damage.

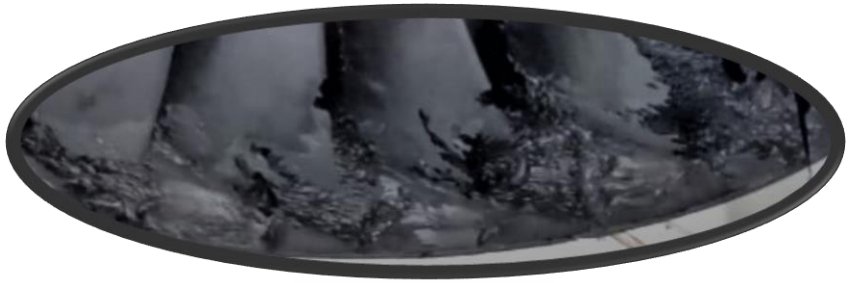

Figure 5.2 Highlighted penetrated/prone area of the blade due to cavitation effect

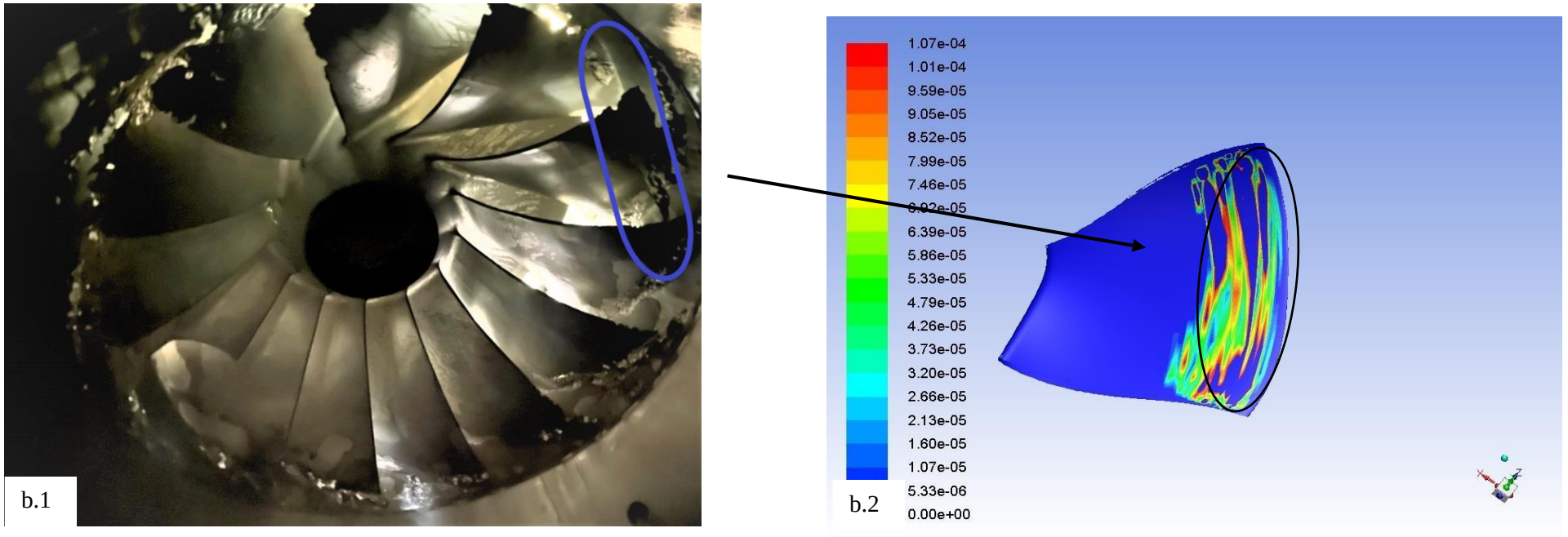

Figure 5. 3 Comparison of the eroded region obtained using erosion rate density parameter of ANSYS Fluent with the actually affected/eroded model

Figure 5.3 (b.1) is the eroded model of Kali Gandaki "A" Hydroelectric Plant (144MW) **(Cr: Mr Binod Pandey, an NEA Engineer)**; here material loss as well as portion of the blade along the lower part of trailing edge found missing. Similar pattern of erosion were observed when we performed the simulation in ANSYS Fluent Multiphase Eulerian Dense Discrete phase model. The area that is highly affected by the quartz particle is noted along the trailing edge pressure side of blade profile. The area marked by the circle in figure 5.3 (b.2) indicates the location of the erosion damage.

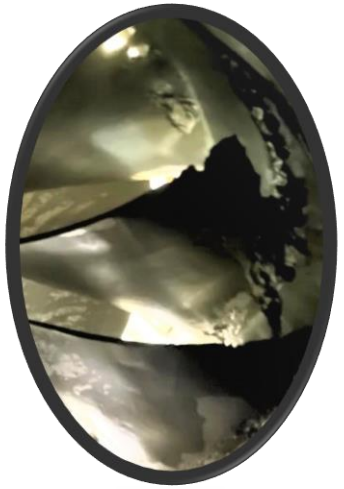

Figure 5. 4 Highlighted portion of the blade missing of the blade due to combined effect

CHAPTER 6 CONCLUSION AND RECOMMENDATIONS

6.1 Conclusion

The outcomes of the CFD simulations have significantly enhanced our understanding of the complex and multiphase phenomena of cavitation and sediment erosion. ANSYS Fluent 19.2 was employed to look into both the individual effects of cavitation and sediment erosion and their combined impact. This simulation has proven valuable in identifying critical areas susceptible to cavitation, sediment erosion, and their interplay.

From the simulation result, it is found that in medium head turbines, erosion rate density is less significant; equal to 1.63E-08 $kgm^{-2}s^{-1}$ for BEP, as compared to high head power plants as velocity of water at the runner is low comparatively as erosion rate is proportional to third power of the velocity. However, cavitation is observed to be more likely because there are more vapor bubbles generated at the runner blades' trailing edge (suction side). Therefore, in a medium head Francis turbine, trailing edge cavitation along the suction side of the runner when low pressure is noticed along that region may be decreased by altering the runner blade's lean angle. Additionally, it finds that the combined condition estimates an erosion rate density on runners of 7.52E-05 $kgm^{-2}s^{-1}$, which is 4.61×10^{3} times higher than the erosion rate density found when examining the effect of sediment erosion only at BEP.

Comparing the results, it is evident that the region where the Kali Gandaki "A" Hydroelectric Plant (HEP) runner experienced critical material loss and missing blade parts aligns precisely with the region predicted by simulating the process in ANSYS Fluent using the Multiphase Eulerian Dense Discrete Phase model. Sediment-water-vapor has a significant effect on the trailing edge of the blade profile, impacting both the suction side and the pressure side and causing material loss at that particular spot.

6.2 Recommendations

Following things can be recommended for further works in the field:

- Researchers should concentrate on quartz particle shapes as well because they have a significant impact on erosion rates.
- To precisely determine the smooth operational duration of the runner and to forecast the maintenance time of the runner, the researcher should advance their research on the material loss rate.

REFERENCES

Agrawal, M. (Director). (2012). *Erosion Modeling and Sand Management with ANSYS CFD, Presentation Slide [Motion Picture]*.

Anmol Mukhia, X. Z. (2021, October). Nepal's hydropower development: Predicament. Natural Resources Forum.

ANSYS Fluent 12.0 Theory Guide-16.7.4 Cavitation Models. (n.d.). Retrieved from https://www.afs.enea.it/project/neptunius/docs/fluent/html/th/node343.htm

Avellan, F. (2004). Introduction to Cavitation in Hydraulic Machinery. *The 6th international Conference on Hydraulic Machinery and Hydrodynamics* (pp. 11-22). Timisoara, Romania: Scientific Bulletin of the Politehnica University of Timisoara.

B S Thapa, B. T. (2012). Optimizing runner blade profile of Francis turbine to minimize sediment erosion. *IOP Conference Series: Earth and Environmental Science 15.*

Balendra Chhetry, K. R. (2015). Effect on Sand erosion on Turbine Components: A Case Study of Kaligandaki "A" HEP-144MW, Nepal. *Hydro Nepal Journal of Water Energy and Environment* .

Bhola Thapa, R. S. (27 December 2015). Problems of Nepalese hydropower projects due to suspended sediments. *Aquatic Ecosystem Health and management*, 251-257.

Biraj Singh Thapa, B. T. (2012). Empirical modelling of sediment erosion in Francis turbines. *Energy; The International Journal*, 386-391.

Brennen, C. (2011). *Hydrodynamics of pumps.*

Chitrakar, S. (June, 2018). *Secondary Flow and sediment erosion in Francis turbines* . NTNU: Doctorate Degree.

Daoyin Liu, C. B. (2013). Development and test of CFD-DEM model for complex

geometry: A Coupling algorithm for Fluent and DEM. *Computer and Chemical Engineering*, 260-268.

Elyyan, M. (Director). (2017). *Better particle Erosion Fluid Dynamics Modeling in ANSYS Fluent 18, Fluid Dynamics, Tips and Tricks* [Motion Picture].

Gjosaeter, K. (2011). *Hydraulic Design of Francis Turbine Exposed to sediment Erosion.* NTNU: Master Thesis.

Glover, D. K. (2003). Hydropower Development. *Hydraulic Design*, pp. 8-10.

H.P.Neopane. (2010). *Sediment erosion in Hydro Turbines.* NTNU.

Initiative, S. A. (n.d.). *International Hydropower Association*. Retrieved from Sediment Management: https://www.hydropower.org/sediment-management-case-studies/nepal-kali-gandaki

Md Rakibuzzaman, H.-H. K.-H. (7 March 2019). Numerical Study of Sediment Erosion Analysis in Francis Turbine. *Sustainability*.

Min- Woo Kang, N. P.-H. (2016). Numerical study on sediment erosion of Francis turbine with different operating conditions and sediment inflow rates. *IX International Conference on computational Heat and Mass Transfer* (pp. 457-464). Procedia Engineering.

NEA. (2022/2023). *Annual Report.* Durbar Marg, Kathamndu, Nepal.

Neopane, H. a. (2011). Sediment erosion in hydraulic turbine. *Global J Res Eng*, 17-26.

Poudel, L. (2012). Effect of Sediment Size in Hydraulic Turbine Material: A Case Study of Roshi Khola in Nepal. *Nepal Journal of Science and Technology*, 129-132.

R. Lama, D. R. (2018). Numerical investigation on performance and sediment erosion of Francis runner with different guide vane profiles. *Journal of Physics: Conference Series*.

R. Manandhar, B. S. (2019). *Numerical Investigation of sediment erosion and cavitation in francis turbine.*

S. Sangal, M. S. (2018). Hydro-abrasive erosion in hydro turbines: a review. *Int. J. Green Energy*, (pp. 232-253).

Saeed, R. A. (2015). Numerical Simulation of Three-Dimensional Cavitating Turbulent Flow in Francis turbine with ANSYS. *Int. J. Mech. Aerospace, Ind. Mechatron. Manuf.. Eng.*, 1539-1544.

Saini, P. G. (2016). Numerical study of cavitation inn francis turbine of a small hydro power plant. *J. Applied Fluid Mech.*, 357-365.

Shrestha, S. D. (2020). Numerical Modelling of Hydraulics and Sediment at the Headworks of Kali Gandaki A Hydropower Plant, Nepal. NTNU.

Srinivasan, V. (Director). (2014). Simulating Erosion using ANSYS Computational Fluid Dyanamics, Phd Senior Technical Service Engineer, Presentation slide [Motion Picture].

Stevens, K. (ide/9889567/,n.d.). SlidePlayer. Retrieved from ANSYS: BladeModeler: https://slideplayer.com/sl

Subramanya, K. (2013). *Hydraulic Machines.* Tata McGraw Hill.

Thapa, B. (2004). *Sand Erosion in Hydraulic Machinery.* NTNU: Doctoral thesis .

Thapa, B. S. (2011). Hydraulic Design of Francis Turbine to minimize sediment erosion. *Kathmandu University, Dhulikhel*.

Upadhyay1), B. T. (2007). Study of Combined Effect of Sand Erosion and Cavitation.

X B Zheng, L. L. (2018). Improved Schnerr-Sauer Cavitation model for unsteady cavitating flow on NACA66. *IOP Conference Series.* Earth and Environmental Science.

ANNEX 1: NUMERICAL MODELS AND ADDITIONAL PARAMETERS

Table displaying the models and additional parameters used for the numerical modeling of the sediment erosion effect, the cavitation effect, and their combined for best efficiency point:

S.N	Description	Cavitation	Sediment Erosion	Combined Effect
1	Component	Only one runner blade		
2	Model Used	Mixture Multiphase model	Dense Descrete Phase model	Multiphase Eulerian- Dense Discrete phase model
		Schnerr and Sauer model	All four defult erosion correlation were activated (i.e. Generic, Finnie, Oka and McLaury	Schnerr and Sauer model and Finnie model
3	Turbulence model	SST k-omega model		
4	Defining sediment injection	No injection	Quartz particle with: Density: 2650kg/m3 Diameter: 0.0001m flow rate of sediment: 21.7 kg/s	
5	Inlet parameter	GV angle: 20 degree (BEP) Mass flow rate: 3615.38 kg/s Cylindrical Co-ordinates (a, r, t): (0, -0.34, -0.93) Rotational Speed: -300rpm		
6	Boundary condition's	Inflow: Mass-flow inlet Blade, hub and shroud: Wall Outlet: Pressure outlet		
7	DPM boundary conditions for wall	None	"Reflect" BC at walls "Escape" option for inlet and outlet BC	

ANNEX 2: PLAGIARISM REPORT

STUDY OF CORRELATION BETWEEN CAVITATION AND SEDIMENT EROSION IN FRANCIS TURBINE

ORIGINALITY REPORT

7%
SIMILARITY INDEX

PRIMARY SOURCES

1	Ranjeet Twayna, Ram Manandhar, Bikash Singh, Dadiram Dahal, Atmaram Kayastha, Biraj Singh Thapa. "Numerical investigation of Cavitation in Francis Turbine", IOP Conference Series: Earth and Environmental Science, 2022 Crossref	87 words — 1%
2	www.researchgate.net Internet	73 words — 1%
3	fdocuments.net Internet	56 words — 1%
4	Pankaj Gohil, Rajeshwer Saini. "Numerical Study of Cavitation in Francis Turbine of a Small Hydro Power Plant", Journal of Applied Fluid Mechanics, 2016 Crossref	54 words — 1%
5	Pankaj P. Gohil, R.P. Saini. "Coalesced effect of cavitation and silt erosion in hydro turbines—A review", Renewable and Sustainable Energy Reviews, 2014 Crossref	51 words — < 1%
6	Sarkar, Snigdha. "Numerical Investigation of Vapor and Gaseous Cavitation in Squeeze-Film Damper Bearings.", University of Cincinnati, 2018 ProQuest	39 words — < 1%

7	www.ansys.com Internet	33 words —	< 1%
8	Escaler, X.. "Detection of cavitation in hydraulic turbines", Mechanical Systems and Signal Processing, 200605 Crossref	31 words —	< 1%
9	mafiadoc.com Internet	28 words —	< 1%
10	R.S. Amano, N.F. Rieger, S. Hesler. "An aerodynamic analysis of turbine cascade by using a second-order closure of turbulence", International Journal of Heat and Fluid Flow, 1996 Crossref	24 words —	< 1%
11	ijamtes.org Internet	23 words —	< 1%
12	Subhash N. Shah, Samyak Jain. "Coiled tubing erosion during hydraulic fracturing slurry flow", Wear, 2008 Crossref	20 words —	< 1%
13	Chirag Sedani, Paritosh Chaudhuri, Manoj Kumar Gupta. "Heat transfer and fluid flow analysis of pebble bed and its verification with Artificial neural network", Nuclear Materials and Energy, 2023 Crossref	19 words —	< 1%
14	K R Rakeshasharma, M K Padhy, Abhilipsa Hota, S K Sarangi. "A literature survey on silt erosion and cavitation in hydro turbine", 2016 International Conference on Signal Processing, Communication, Power and Embedded System (SCOPES), 2016 Crossref	19 words —	< 1%

15 Feng Hong, Hailin Tian, Xi Yuan, Shuchang Liu et al. "CFD-assisted modeling of the hydrodynamic cavitation reactors for wastewater treatment — A review", Journal of Environmental Management, 2022
Crossref
18 words — < 1%

16 Mahmoud A. El-Emam, Ling Zhou, Eman Yasser, Ling Bai, Weidong Shi. "Computational Methods of Erosion Wear in Centrifugal Pump: A State-of-the-Art Review", Archives of Computational Methods in Engineering, 2022
Crossref
18 words — < 1%

17 Rafael Campos-Amezcua, Sofiane Khelladi, Zdzislaw Mazur-Czerwiec, Farid Bakir, Alfonso Campos-Amezcua, Robert Rey. "Chapter 8 Numerical and Experimental Study of Mass Transfer Through Cavitation in Turbomachinery", IntechOpen, 2011
Crossref
18 words — < 1%

18 Kwang-Yong Kim, Abdus Samad, Ernesto Benini. "Design Optimization of Fluid Machinery", Wiley, 2019
Crossref
14 words — < 1%

19 Thapa, B S, B Thapa, M Eltvik, K Gjosater, and O G Dahlhaug. "Optimizing runner blade profile of Francis turbine to minimize sediment erosion", IOP Conference Series Earth and Environmental Science, 2012.
Crossref
14 words — < 1%

20 www.freepatentsonline.com
Internet
14 words — < 1%

21 Namdev Dhas, Hosadurga Shantharam Preetha, Akhilesh Dubey, Gundawar Ravi et al. "Factorial design-based fabrication of biopolymer-functionalized Asiatic
13 words — < 1%

acid-embedded liposomes: in-vitro characterization and evaluation", Journal of Applied Pharmaceutical Science, 2022
Crossref

22 docplayer.net
Internet
11 words — < 1%

23 Hanafizadeh, Pedram, S. Alireza Hojati, Hamid Eslami, and Navid Latifian. "High Reynolds Gas-Liquid Two Phase Flow Around a Triangular Body", Volume 2 Dynamics Vibration and Control Energy Fluids Engineering Micro and Nano Manufacturing, 2014.
Crossref
9 words — < 1%

24 Jose, July Kooran. "Modeling Cavitation in a High Intensity Agitation Cell", Proquest, 20111109
ProQuest
9 words — < 1%

25 dspace.unza.zm
Internet
9 words — < 1%

26 eprints.utm.my
Internet
9 words — < 1%

27 Anastasios N. Georgoulas, Kyriakos I. Kopasakis, Panagiotis B. Angelidis, Nikolaos E. Kotsovinos. "Numerical investigation of continuous, high density turbidity currents response, in the variation of fundamental flow controlling parameters", Computers & Fluids, 2012
Crossref
8 words — < 1%

28 Greg A. Valentine. "Multifield governing equations for magma dynamics", Geophysical & Astrophysical Fluid Dynamics, 1994
Crossref
8 words — < 1%

29 Odabaee, Mostafa, Sauret, Emilie, Hooman, Kamel. "Computational fluid dynamics simulation
8 words — < 1%

and turbomachinery code validation of a high pressure ratio radial-inflow turbine", HEFAT / University of Pretoria, 2014
Internet

30 Yuxiu Liang, Fushui Liu, Yikai Li, Xiaodong An. "Research on the Dynamic Cavitation Flow Characteristics in the Control Valve Region during the Opening Process of the Valve in an Electronic Unit Pump", IEEE Access, 2020 — 8 words — < 1%
Crossref

31 Antoine Ducoin, Ramona B. Barber, Stuart J. Wildy, John D. Codrington, Aaron Baker. "Experimental evaluation of the use of embedded fiber Bragg gratings to measure steady and unsteady flow-induced marine propeller blade deformation", Ocean Engineering, 2023 — 7 words — < 1%
Crossref

32 Jablonsk, J.. "Modelling on cavitation in a diffuser with vortex generator", EPJ Web of Conferences, 2013. — 6 words — < 1%
Crossref

EXCLUDE QUOTES	ON	EXCLUDE SOURCES	OFF
EXCLUDE BIBLIOGRAPHY	ON	EXCLUDE MATCHES	OFF